Figure 4. Comparison of in vivo tumorigenicity of ALDH1^{high} cells and ALDH1^{low} cells. A ALDH1$^{high/low}$ tumors derived from AMOC-2 cells. B ALDH1$^{high/low}$ tumors derived from RMG-1 cells. Picture: NOD/SCID mice that were injected with 1.0×10^3 ALDH1$^{high/low}$ cells and in which tumors observed on both sides of their back. Histological images: Hematoxylin-Eosin staining (H-E, left panel), ALDH1 immunohistochemical staining (middle panel), Ki-67 immunohistochemical staining (right panel) of ALDH1$^{high/low}$ tumors. Magnification of images: × 400. **C Growth curves of ALDH1$^{high/low}$ tumors derived from AMOC-2 and RMG-1 cells.** Left column: AMOC-2 cells, 1.0×10^3 injection. Middle column: AMOC-2 cells,1.0×10^2 injection. Right column: RMG-1 cells, 1.0×10^3 injection. Each value is the mean tumor volume ± SD. *P values. **D Immunoreactivity to ALDH1 or Ki-67 of ALDH1$^{high/low}$ tumors derived from AMOC-2 and RMG-1cells** Each value is the mean positive percentage ± SD. *P values.
doi:10.1371/journal.pone.0065158.g004

Technologies) until separated into single cells. The cells obtained by these procedures were analyzed by flow cytometry as described below.

ALDEFLUOR Assay and Isolation by Fluorescence-activated Cell Sorting (FACS)

We used an ALDEFLUOR assay kit (Stem Cell Technologies^{TM}, Vancouver, BC, Canada) to determine ALDH1 activity of cells according to the manufacturer's protocol. Cells were suspended in ALDEFLUOR assay buffer containing 1 μmol/l per $1x10^6$ cells of the ALDH substrate, boron-dipyrromethene-aminoacetaldehyde (BAAA), and incubated for 50 min at 37°C. Each sample was treated with 50 mmol/l of an ALDH-specific inhibitor, diethylaminobenzaldehyde (DEAB), as a negative control. Stained cells were analyzed by BD FACSAria^{TM} II (BD Biosciences, San Jose, CA, USA). Cells were stained with 1 μg/ml of propidium iodide to evaluate their viability prior to analysis.

For isolation of epithelial cells from solid ovarian cancer specimens, we sorted epithelial cancer cells using anti-CD326 (Ep-CAM) APC antibody (BD Biosciences). We used anti-CD326 microbeads (BD Biosciences) and an Automacs system (Miltenyi Biotec, Bergisch Gladbach, Germany) to enrich epithelial cells from malignant ascites of ovarian cancer cases before the ALDEFLUOR assay.

Cell Cycle Analysis and *in vitro* Cell Grow Analysis

ALDH1^{high} and ALDH1^{low} cells were directly fixed with 70% ethanol after sorting. Then they were resuspended in PBS containing 250 μg/ml RNase A (Sigma-Aldrich) for 30 minutes at 37°C and stained with 50 μg/ml propidium iodide for 10 minutes at 4°C in the dark. Stained cells were analyzed with a FACSCalibur (BD Biosciences), and the data were analyzed using the Mod-Fit cell cycle analysis program.

For *in vitro* cell growth assay, ALDH1^{high} cells and ALDH1^{low} cells isolated from AMOC-2 and RMG-1 cells were seeded into a 6-well plate at 5×10^4 cells per well. After incubation for 48 and 96 hours, the cells were removed by trypsin and viable cell numbers were determined using Countess® (Life Technologies).

Sphere-forming Assay/single Cell Sphere-forming Assay

ALDH1^{high} and ALDH1^{low} cells were isolated by FACS and then cultured in 6-well ultra-low attachment surface dishes (Corning, Tewksbury, MA, USA) at 1000 cells per well. For the single cell sphere-forming assay, both ALDH1^{high} and ALDH1^{low} were sorted into 96-well ultra-low attachment dishes (Corning) at a single cell per well. The cells were cultured in stem-cell medium, serum-free DMEM/F12 (Life Technologies) supplemented with N-2 supplement (Life Technologies), 20 mg/ml recombinant human epithelial growth factor (Life Technologies), 10 mg/ml human basic fibroblast growth factor (Sigma-Aldrich), 4 μg/ml heparin (Sigma-Aldrich), 4 mg/ml bovine serum albumin (Life Technologies), 20 g/ml human insulin, zinc solution (Life technologies), and 2.9 mg/ml glucose (Sigma-Aldrich). [29] Morphological change was observed daily under a light microscope for 14 days.

In vivo Tumorigenicity

Sorted ALDH1^{high} and ALDH1^{low} cells were resuspended at 1.0×10^2, 1.0×10^3 and 1.0×10^4 cells in 100 μl PBS and Matrigel (BD Biosciences) mixture (1:1). Then each mixture was injected subcutaneously into the right/left middle back areas of 6-week-old female non-obese diabetic/severe combined immune-deficiency (NOD/SCID) mice (NOD.CB17-Prdkcscid/J, Charles River Laboratory, Yokohama, Japan) under inhalation anesthesia by isoflurane. Tumor initiation and progression were observed weekly until the mice were sacrificed at 7 weeks after injection. External tumor volume was calculated as $0.5\times$ Dmax$\times$ (Dmin)^2 [mm^3] (Dmax : long axis, Dmin : short axis of mass).

Immunohistochemical Staining for Ovarian Cancer Tissue

Immunohistochemical staining of ALDH1 and Ki-67 was performed with formalin-fixed, paraffin-embedded sections of 123 epithelial ovarian cancer tissues (62 serous adenocarcinomas, 37 clear cell adenocarcinomas, 18 endometrioid adenocarcinomas and 6 mucinous adenocarcinomas) as described previously. [30] [31] Antigen retrieval was done by boiling sections in 120°C for 5 min in a microwave oven in preheated 0.01 mol/l sodium citrate (pH 6.0). Endogenous peroxidase activity was blocked by 3% hydrogen peroxide in ethanol for 10 min. After blocking with 1% non-fat dry milk in PBS (pH 7.4), the sections were reacted

Table 1. Tumor-initiation incidence of ALDH1$^{high/low}$ cells derived from AMOC-2 and RMG-1 cells.

	AMOC-2		RMG-1	
Number of cells injected into mice	**ALDH1^{high}**	**ALDH1^{low}**	**ALDH1^{high}**	**ALDH1^{low}**
1.0×10^4	5/5	3/5	4/5	2/5
1.0×10^3	4/5	2/5	3/5	2/5
1.0×10^2	2/5	0/5	0/5	0/5

The number indicates the incidence of tumor-initiation of NOD/SCID Mice.
doi:10.1371/journal.pone.0065158.t001

Table 2. Patient list of clinical specimen that were examined by ALDEFLUOR assay.

Cancer cells from solid cancer tissue					
Pt.No.	**Age**	**Histological subtype**	**Stage**	**ALDH1^{high}**	**CD326+[%]**
1	42	Clear	Ic	7.2	62.7
2	67	Mucinous	IIIc	0	16.5
3	52	Endometrioid	Ic	12	78.7
4	45	Clear	Ic	8.1	8.1
5	71	Serous	IIIc	2.2	80
Mean	55.4			4.46	49.2
±SD	±13.0			±5.05	±34.5
Cancer cells from ascites					
Pt.No.	Age	Histological subtype	Stage	ALDH1^{high}	
1	65	Unknown	IIIc	0	
2	62	Serous	IIIc	2.2	
3	67	Mucinous	IIIc	0	
4	58	Serous	IIIc	4.2	
5	52	Serous	IIIc	4.1	
6	59	Clear+Endometrioid	IIIb	1.7	
Mean	60.5			2.03	
±SD	±5.39			±1.86	

Cancer cell from primary cancer tumor : 6 cases/Cancer cell from ascites : 5 cases.

doi:10.1371/journal.pone.0065158.t002

with mouse anti-ALDH1 monoclonal antibody (1:250, Sigma-Aldrich) or mouse anti-Ki-67 monoclonal antibody (1:100, DAKO, Glostrup, Denmark) for 1 hour followed by incubation with biotinylated anti-mouse IgG (Nichirei) for 30 min. Subsequently, the sections were stained with setreptavidin-biotin complex (Nichirei Biosciences, Tokyo, Japan), followed by incubation with 3,3′–diaminobenzidine used as a chromogen and counter-staining with hematoxylin. Cytoplasmic staining was regarded as positive for ALDH1, and nuclei staining were regarded as positive for Ki-67. For evaluation of ALDH1 staining, the cases were divided into two groups (ALDH1^{high} group and ALDH1^{low} group) by medians (medians for serous adenocarcinoma the median and clear cell adenocarcinoma being 20% and 15%, respectively).

Matrigel Invasion Assay

The invasive capability of cells was evaluated using matrigel invasion chambers (BD Biosciences). Isolated ALDH1^{high} and ALDH1^{low} cells (1.0×10^4) were plated in each upper chamber in serum-free DMEM. The outer chambers were filled with DMEM including 10% FBS as a chemoattractant. Cells were incubated for 48 hours, and invasive cells were stained with Hematoxylin, mounted on slides, and counted at 400-fold upper field by light microscopy.

Statistical Analysis

Statistical analysis, data fitting and graphics were performed using SPSS software package ver.19 (SPSS, Chicago, IL, USA). Data are shown as mean ± *SD* of at least 3 independent experiments, and Student's t-test was used to assess statistically significant differences ($p<0.05$). Overall survival (OS), defined as interval from the date of first diagnosis to the date of death from disease progression, and progression-free survival (PFS), defined as the interval from the date of first diagnosis to the date of disease progression, were estimated using the Kaplan-Meier method and compared using the log-rank test. Associations of ALDH1 expression with clinical stage, lymph node metastases and dissemination were analyzed by Fisher's test.

Results

Isolation of ALDH1^{high} Cells from EOC Cell Lines

Several methods to isolate CSCs/CICs have already been described [12], and an aldehyde dehydrogenase 1 high population (ALDH1^{high}) identified by the ALDEFLUOR assay was described to be enriched with CSCs/CICs. [20] We therefore analyzed ovarian carcinoma cell lines by the ALDEFLUOR assay to isolate ovarian CSCs/CICs. We investigated 3 human ovarian serous adenocarcinoma cell lines (AMOC-2, HUOA and OVCAR-3) and 3 human clear cell adenocarcinoma cell lines (ES-2, RMG-1 and TOV-21G) (Figure 1). ALDH1^{high} population was identified in all ovarian carcinoma line cells, and the ratio of ALDH1^{high} cells ranged from 0.7% for ES-2 cells to 7.9% for TOV-21G cells. We could isolate ALDH1^{high} cells stably from 4 cell lines (AMOC-2, ES-2, RMG-1 and TOV-21G), and we therefore used these cell lines for further analysis.

Characterization of ALDH1^{high} Cells

Since CSCs/CICs are known to form spheres in floating culture conditions [29], we analyzed ALDH1^{high} cells by a sphere-forming assay. A total of 10^3 cells per well were sorted and incubated into a 6–well plate in an anchorage-independent environment. At day 10, ALDH1^{high} cells derived from AMOC-2 cells showed greater sphere-forming ability than that of ALDH1^{low} cells. Similar results were obtained from ES-2 cells, RMG-1 cells and TOV-21G cells (Figure 2A). Since the sphere-forming assay is not suitable for quantification of the ratios of CSCs/CICs in ALDH1^{high} cells, we performed a single cell sphere-forming assay. Sphere formation was observed in 4.86% of the wells of ALDH1^{high} cells derived from AMOC-2 cells and in 3.13% of the wells of ALDH1^{high} cells derived from ES-2 cells (Figure 2B). On the other hand, wells of ALDH1^{low} cells derived from both AMOC-2 and ES-2 cells did not show any sphere formation.

We then investigated the invasion ability of ALDH1^{high} and ALDH1^{low} cells by the matrigel invasion assay. ALDH1^{high} cells derived from all four line cells showed greater matrigel invading ability than did ALDH1^{low} cells (Figure 2C).

The cell cycle status of ALDH1^{high} cells and that of ALDH1^{low} cells were analyzed. The ratios of ALDH1^{high} cells in S phase and G2/M phase were greater than ratio of ALDH1^{low} cells in S phase and G2/M phase (Figure 3A). Cell grow analysis revealed that ALDH1^{high} cells derived from AMOC-2 and RMG-1 cells had higher grow rates than those of ALDH1^{low} cells (Figure 3B).

Higher Tumorigenicity of ALDH1^{high} Cells than that of ALDH1^{low} Cells

To address the *in vivo* tumorigenicity of ALDH1^{high} and ALDH1^{low} cells from EOC cell lines, xenograft transplantation into NOD/SCID mice by ALDH1^{high} and ALDH1^{low} cells derived from AMOC-2 and RMG-1 cells was performed (Figure 4A, 4B and 4C). As shown in Table 1, tumors were observed in 5 of 5 mice (10^4 cells injection), 4 of 5 mice (10^3 cells injection) and 2 of 5 mice (10^2 cells injection) in which xenotransplantation of ALDH1^{high} cells derived from AMOC-2 cells was performed. On the other hand, tumors were observed in only 3 of 5 mice (10^4 cells injection) and 2 of 5 mice (10^3 cells

Table 3. Correlation between ALDH1 expression and clinical factors in 123 epithelial ovarian cancer patients.

All cases				
Characteristic	**ALDH1^{high}**	**ALDH1^{low}**	**Total**	**P Value**
Patient No.(%)	72(58.5)	51(41.5)	123	
Mean Age ±SD	53.8	50.6	54.8	
[years]	±7.86	±10.7	±10.9	
Pathological				
subtype No.(%)				0.004
Serous	34(54.8)	28(45.2)	62	
Clear cell	18(48.6)	19(51.4)	37	
Endometrioid	14(77.8)	4(22.2)	18	
Mucinous	6(100)	0(0)	6	
FIGO stage No.(%)				0.706
StageI	26(61.9)	16(38.1)	42	
StageII	2(33.3)	4(66.7)	6	
StageIII	39(58.2)	28(41.6)	67	
StageIV	5(62.5)	3(37.5)	8	
Serous adenocarcinoma				
Characteristic	ALDH1^{high}	ALDH1^{low}	Total	P Value
Patient No.(%)	34(54.8)	28(45.2)	62	
Mean Age ±SD	57.3	55.8	56.6	
[years]	±11.1	±11.9	±11.4	
FIGO stage No.(%)				0.991
I+II	6(60.0)	4(40.0)	10	
III+IV	28(53.8)	24(46.2)	52	
T No.(%)				0.589
T1-2	7(53.8)	6(46.2)	13	
T3	27(55.1)	22(44.9)	49	
Lymphadenectomy				0.537
Case No.(%)	23(53.5)	20(46.5)	43	
L/N Meta (+)				
No. (%)	12(48.0)	13(52.0)	25	
L/N Meta (−)				
No. (%)	11(61.1)	7(38.9)	18	
Clear cell adenocarcinoma				
Characteristic	ALDH1^{high}	ALDH1^{low}	Total	P Value
Patient No.(%)	18(48.6)	19(51.4)	37	
Mean Age ±SD	50.9	53.0	52.2	
[years]	±8.2	±10.1	±9.4	
FIGO stage No.(%)				0.060
I+II	7(30.4)	16(69.6)	23	
III+IV	8(57.1)	6(42.9)	14	
T No.(%)				0.303
T1-2	14(45.2)	17(54.8)	31	
T3	4(66.7)	2(33.3)	6	
Lymphadenectomy				0.071
Case No.(%)	14(46.7)	16(53.3)	30	
L/N Meta (+)				
No. (%)	4(50.0)	4(50.0)	8	

Table 3. Cont.

All cases				
Characteristic	**ALDH1^{high}**	**ALDH1^{low}**	**Total**	**P Value**
L/N Meta (−)				
No. (%)	10(45.5)	12(54.5)	22	

P values calculated by Fisher's test. For all 123 cases, histological subtypes and FIGO clinical stage were investigated about the relevance to ALDH1 expression. Individually in serous or clear cell adenocarcinoma cases, investigated the relevance with ALDH1 expression to FIGO clinical stage, T-classification and lymph nodes metastases.

doi:10.1371/journal.pone.0065158.t003

injection) in which xenotransplantation of ALDH1^{low} cells was performed. Furthermore, growth rate of tumors derived from AMOC-2 ALDH1^{high} cells was significantly faster than that of tumors derived from AMOC-2 ALDH1^{low} cells (Figure 4C). Similar results were obtained for RMG-1 cells (Figure 4B and 4C).

Histological aspects of tumors derived from ALDH1^{high} cells and ALDH1^{low} cells that were isolated from AMOC-2 and RMG-1 cells were investigated (Figure 4A and 4B). Tumors derived from AMOC-2 ALDH1^{high} cells and AMOC-2 ALDH1^{low} cells showed poorly differentiated adenocarcinoma and there was no significant difference. Similarly, tumors derived from RMG-1 ALDH1^{high} cells and RMG-1 ALDH1^{low} cells showed poorly differentiated clear cell adenocarcinoma. Immunohistochemical staining revealed that there was no significant difference in ALDH1-positive rate between tumors derived from AMOC-2 ALDH1^{high} cells and tumors derived from AMOC-2 ALDH1^{low} cells, whereas the tumor derived from RMG-1 ALDH1^{high} cells showed significant higher ALDH1 positive rates than that of tumor derived from RMG-1 ALDH1^{low} cells (Figure 4D). Furthermore, tumors derived from AMOC-2 ALDH1^{high} cells and RMG-1 ALDH1^{high} cells showed significantly higher positive rates for Ki-67 (MIB-1) than those of tumors derived from AMOC-2 ALDH1^{low} cells and RMG-1 ALDH1^{low} cells (Figure 4D).

Identification of ALDH1^{high} Cells in Primary EOC Samples

To detect ALDH1^{high} cells in primary ovarian cancer, we analyzed eleven clinical materials using the ALDEFLUOR assay (5 cases of solid ovarian cancer cells and 6 cases of malignant ascites of ovarian cancer cases, summarized in Table 2). CD326-positive epithelial cells were identified in solid ovarian cancer tissues, and the positive rates ranged from 8.1% to 81.0% (Figure 5A, upper panels). ALDH1^{high} cells were detected in 4 of the 5 cases, and positive ALDH1^{high} cell rates ranged from 0.9% to 12.0% (Figure 5A, lower panels). Furthermore, ALDH1^{high} cells were detected in CD326-positive cells derived from ovarian cancer ascites in 4 of the 6 cases, and the positive rates of ALDH1^{high} cells ranged from 1.7% to 4.2% (Figure 5B). Therefore, ALDH1 activity determined by using the ALDEFLUOR assay might be a useful approach for isolation of CSCs/CICs from primary ovarian cancer cells.

Association of High Expression Level of ALDH1 is with Poor Prognosis

A total of 123 epithelial ovarian cancer tissues were immunohistochemically stained with anti-ALDH1 antibody (Table 3, Figure 6A). The medians of ALDH1-positive rates in serous adenocarcinoma cases and clear cell adenocarcinoma cases were 20% and 15%, respectively. We therefore divided the cases into

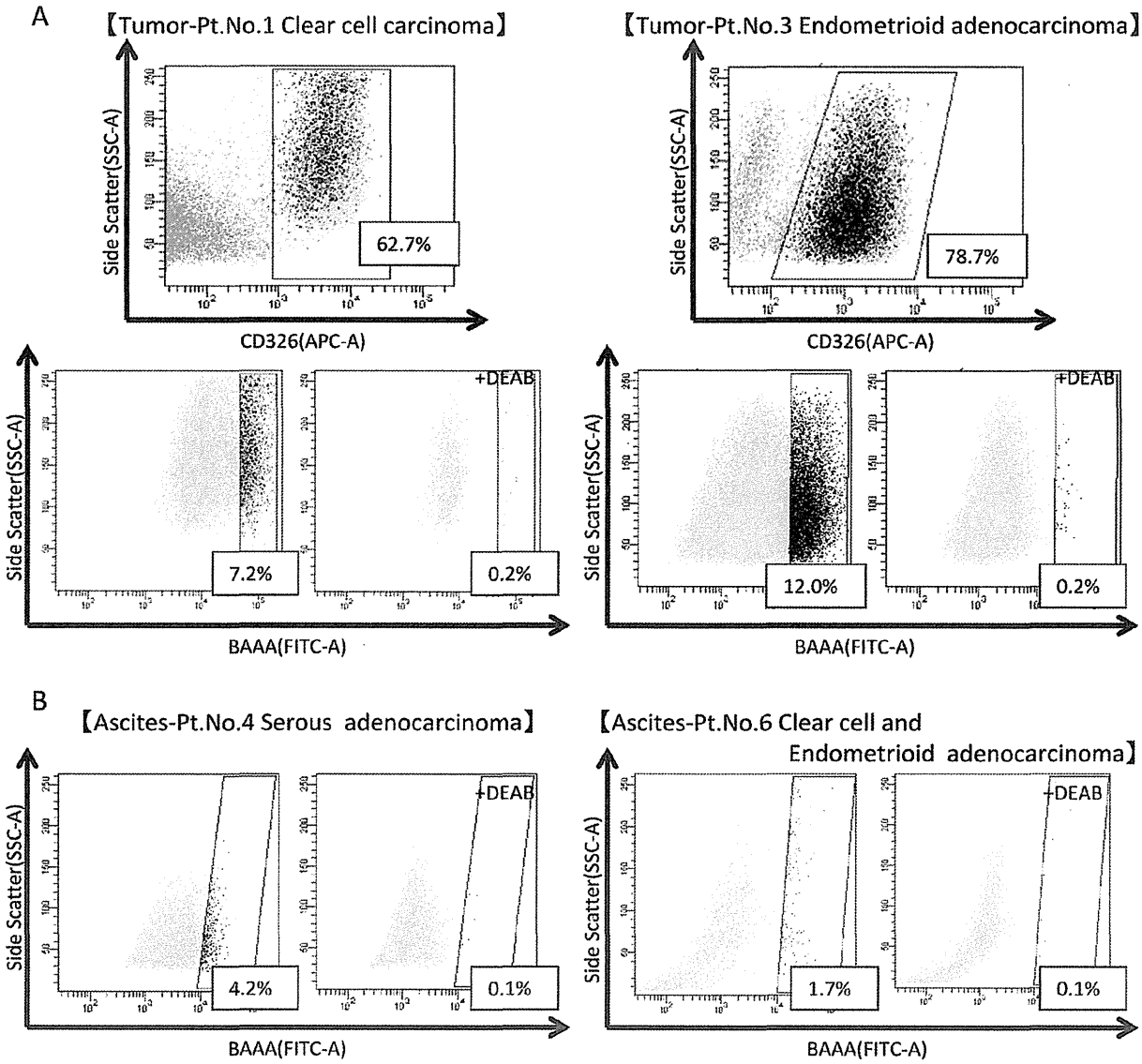

Figure 5. ALDEFLUOR assay for primary solid ovarian cancer cells or cancer cells in ascites. A Analysis of primary solid ovarian cancer cells Upper panel shows CD326 staining. Percentage indicat positive rate for CD326 cells. Lower panel shows ALDEFLUOR assay of CD326-positive cells. Left: Patient No.1, case of stage Ic clear cell adenocarcinoma. Right: Patient No.3, case of stage Ic endometrioid adenocarcinoma. **B Analysis of primary cancer cells from ascites** CD326-positive selection was done before ALDEFLUOR analysis. Left: Patient No.4, case of stage IIIc serous adenocarcinoma. Right: Patient No.6, case of stage IIIb clear cell and endometrioid adenocarcinoma. CD326: Epithelial cell adhesion molecule (EpCAM). APC: allophycocyanin area. Percent scores in boxes indicate CD326-positive or ALDH1-activity ratios.
doi:10.1371/journal.pone.0065158.g005

two groups, ALDH1^{high} group and ALDH1^{low} group, according to the medians. As shown in Table 3, there was no significant correlation of the expression level of ALDH1 with age or with each FIGO clinical stage. High expression level of ALDH1 showed no significant correlation with advanced stages (stage III+IV), T factor or lymph node metastasis in both serous adenocarcinoma cases and clear cell adenocarcinoma cases. The log-rank test revealed that higher expression level of ALDH1 is associated with poorer prognosis with a significant difference in OS of patients with serous adenocarcinoma ($P = 0.006$) and OS of patients with clear cell adenocarcinoma ($P = 0.047$) than those of lower expression level of ALDH1 (Figure 6B). Higher expression level of ALDH1 showed a tendency for shorter PFS than that of lower expression level of ALDH1, but the differences were not significant (serous adenocarcinoma: $P = 0.062$; clear cell adenocarcinoma: $P = 0.058$).

Discussion

In this study, we isolated ovary CSCs/CICs with high tumorigenicity by the ALDEFLURO assay. An ALDH1^{high} population could be isolated not only from ovarian cancer cell

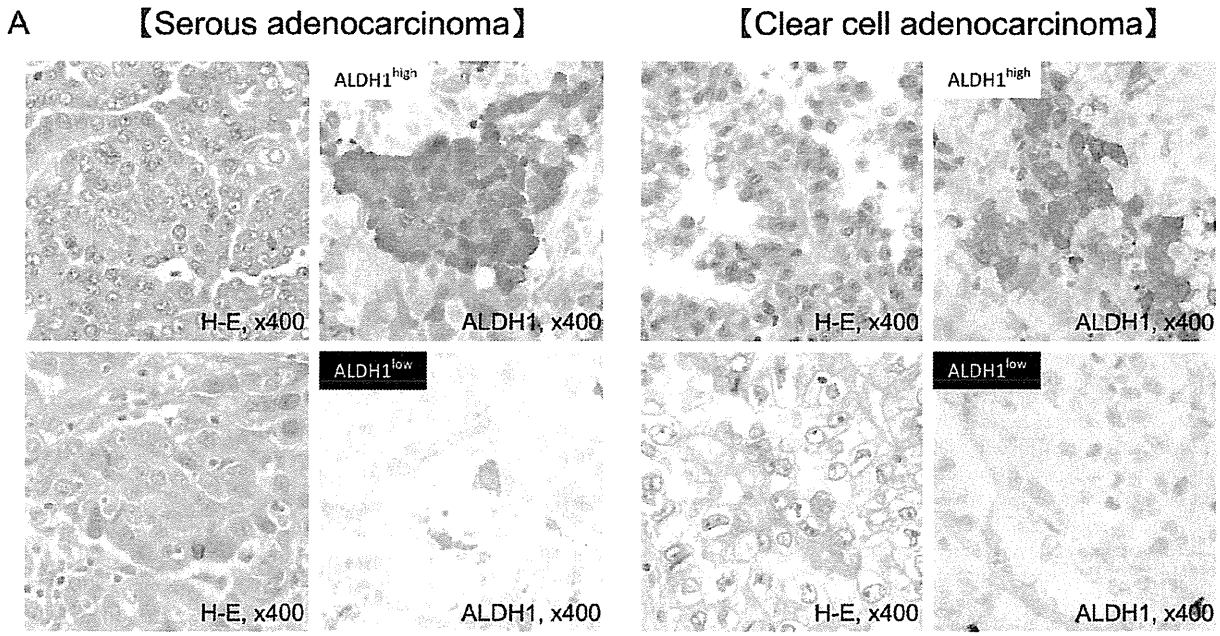
A
【Serous adenocarcinoma】
【Clear cell adenocarcinoma】
ALDH1high
H-E, x400
ALDH1, x400
ALDH1low

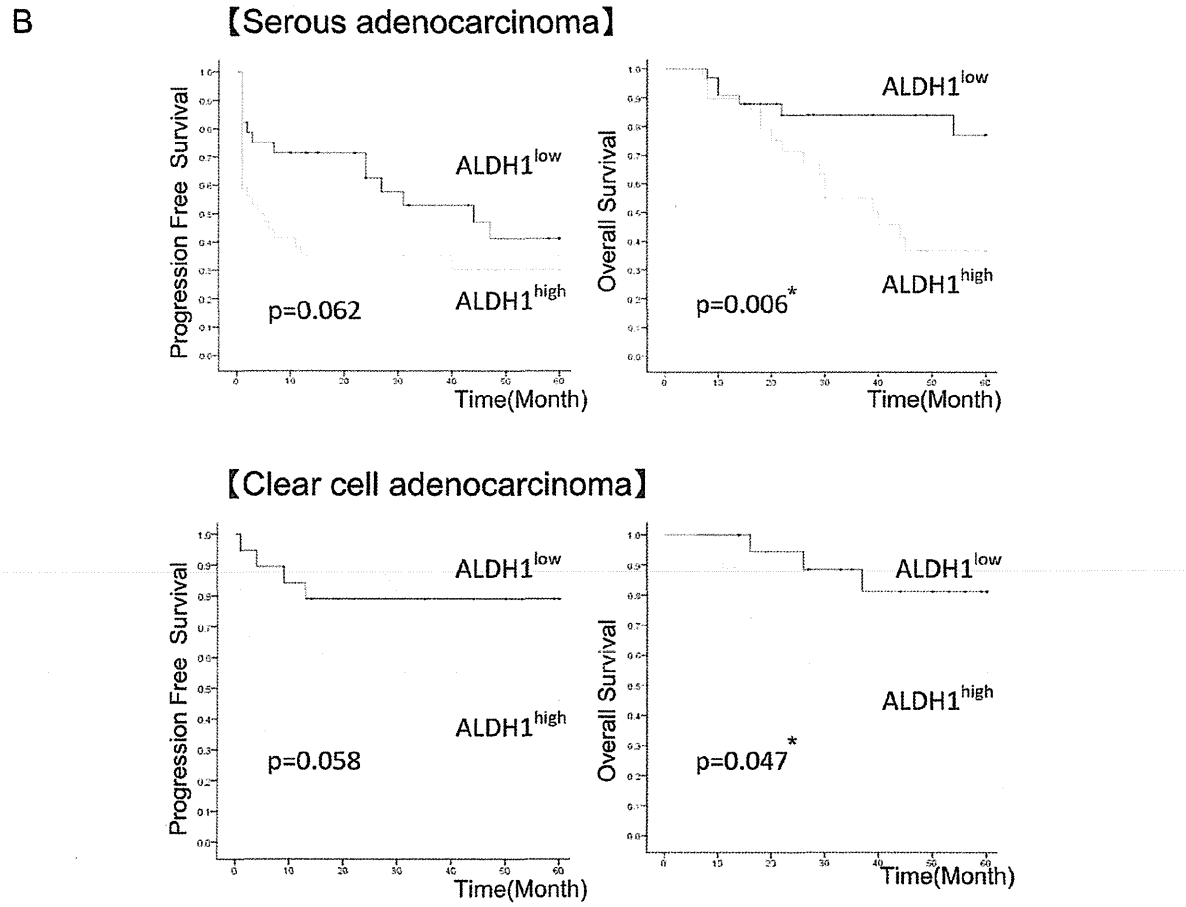
B
【Serous adenocarcinoma】
Progression Free Survival
Overall Survival
ALDH1low
ALDH1high
p=0.062
p=0.006*
Time(Month)
【Clear cell adenocarcinoma】
p=0.058
p=0.047*

Figure 6. Correlation between ALDH1 immunoreactivity and patients' clinical outcome in ovarian serous and clear cell carcinoma. A H-E staining and ALDH1 immunohistochemical staining of primary ovarian serous adenocarcinoma (left) and primary ovarian clear cell adenocarcinoma (right) Upper left panel: H-E staining of ALDH1^{high} specimen. Upper right panel: ALDH1 immunohistochemical staining of ALDH1^{high} specimen. Lower left panel: H-E staining of ALDH1^{low} specimen. Lower right panel: ALDH1 immunohistochemical staining of ALDH1^{low} specimen. Magnification of images: ×400. **B Log-rank test for ALDH1$^{high/low}$ groups of ovarian serous adenocarcinoma and clear cell adenocarcinoma patients.** Serous adenocarcinoma: 62 cases/clear cell adenocarcinoma: 37 cases. Cases in the ALDH1^{high} group are cases with positive ratio for ALDH1 of over 20% for serous adenocarcinoma cases and 15% for clear cell adenocarcinoma cases. Left: column: progression-free survival (PFS). Right column: overall survival (OS). *P values.
doi:10.1371/journal.pone.0065158.g006

lines but also from primary ovarian cancer samples. Several methods for isolation of CSCs/CICs have been reported. Indeed, ovarian CSCs/CICs have been successfully isolated by using various methods including the ALDEFLUOR assay [25], side population (SP) analysis [32,33], and use of CD133^{+} [34], CD44^{+}CD24^{-} [35] and CD24^{+} cells. [36] However, there is a controversial report showing that a CSC/CIC marker does not work in some types of cells. [37,38] Therefore, it is essential to validate the cell population isolated by CSC/CIC markers by several types of analysis. In this study, we confirmed that the ALDH1^{high} population had higher tumorigenicity and greater sphere-forming ability. These observations indicate that the ALDH1^{high} cells we used in this study are enriched with CSCs/CICs. There have been few reports on successful isolation of CSCs/CICs from primly ovarian cancer cells. We isolated ALDH1^{high} cells from 8 of 11 primary ovarian cancer cases. We could not analyze ALDH1^{high} cells from primary ovarian cancers because of the limitation of cell numbers; however, our approach is a possible and promising method for isolating CSCs/CICs from primary ovarian cancers.

Major histological subtypes of EOC are serous adenocarcinoma, clear cell adenocarcinoma, endometrioid adenocarcinoma and mucinous adenocarcinoma, and these subtypes are known to have different characteristics in risk factor of carcinogenesis, molecular biological aspects and so on. More information about individual subtypes is needed to improve the survival of patients. Serous adenocarcinoma is the histology subtype with worst prognosis; however, serous adenocarcinoma cases are often diagnosed at advanced stage. Clear cell adenocarcinoma is gradually increasing up to nearly 12% of EOC in Asian countries, and comparison of the cases in the same stage of 3 histological subtypes (clear cell adenocarcinoma, endometrioid adenocarcinoma and mucinous adenocarcinoma) revealed that clear cell adenocarcinoma is the poorest prognosis in every stages. Therefore, clear cell adenocarcinoma is thought to be the highest grade EOC, recently. [39,40] Serous adenocarcinoma cases were mainly analyzed in previous studies, and there have been few studies in which clear cell adenocarcinoma cases were analyzed. [23-25] In this study, we analyzed not only serous adenocarcinoma cases but also clear cell adenocarcinoma cases. Therefore, these information will bring insight into not only for serous adenocarcinomas, but also most highest grade clear cell adenocarcinomas.

We found that 4 EOC cell lines including 3 clear cell adenocarcinoma lines were positive for sphere formation with 1000 cells/well. On the other hand, only two cell lines (AMOC-2 and ES-2) showed sphere formation in single cell sphere analysis. These results indicate that CSCs/CICs, which have the ability to form a sphere from only one cell, are enriched in ALDH1^{high} cells; however the ratios of CSCs/CICs are not so high even in ALDH1^{high} populations. This result indicated that the ALDEFLUOR assay is just a surrogate marker for CSCs/CICs and that the combination of ALDEFLUOR assay with other markers might be a better approach to isolate CSCs/CICs.

In previous studies on immunohistochemical staining, contradictory results regarding the association of ALDH1 expression with prognosis in EOC were obtained. Chang *et al.* reported that ALDH1 expression correlates with favorable prognosis in serous or non-serous ovarian carcinoma [26], while Deng *et al.* and Wang *et al.* reported opposite results showing that high ALDH1 activity is linked to poor prognosis in serous adenocarcinoma. [23,25] It should be noted that conditions for immunohistochemical staining and positivity for ALDH1 differed in those studies. In the present study, we set the cut-off lines at 20% for serous adenocarcinoma and 15% for clear cell adenocarcinoma, and we investigated 2 individual histological types. We obtained results showing that high expression level of ALDH1 was associated with poor prognosis in serous and clear cell adenocarcinomas of the ovary. This is the first report showing a relationship between ALDH1 staining and poor prognosis of clear cell adenocarcinomas. On the other hand, ALDH1 expression had no relevance to clinical stage, lymph node metastases or dissemination. These results indicate that ALDH1-positive cells in epithelial ovarian cancer might be responsible for resistance to anti-cancer therapies rather than promotion of diseases. Therefore, ALDH1 might be a novel biomarker for the prediction of prognosis of not only serous adenocarcinoma cases but also clear cell adenocarcinoma cases. Further investigations on molecular aspects of ALDH1^{high} cells in ovarian cancers are needed.

In summary, we successfully isolated an ALDH1^{high} cell population with high tumorigenicity not only from serous adenocarcinoma but also from clear cell adenocarcinoma. ALDH1^{high} cells have higher tumorigenicity and greater sphere-forming ability. ALDH1-positive immunohistochemical staining is related to poor prognosis in both serous adenocarcinoma and clear cell adenocarcinoma. These findings indicate that ovarian CSCs/CICs are positive for ALDH1, and further analysis of ALDH1-positive ovarian CSCs/CICs will lead to the establishment of novel strategies for treating ovarian CSCs/CICs.

Acknowledgments

We thank Dr. Satoshi Tanaka, Dr. Noriyoshi Fukunaka, Dr. Kaori Fukunaka (Hakodate Goryokaku Hospital, Hakodate, Hokkaido, Japan), Dr. Takahiro Suzuki, Dr. Masahiro Iwasaki and Dr. Ryouichi Tanaka (Sapporo Medical University Hospital, Sapporo, Hokkaido, Japan) for providing clinical specimens based on the IRB, and we thank Ms. Eri Saka for technical assistance.

Author Contributions

Conceived and designed the experiments: TK YH TT TS NS. Performed the experiments: TK KY AT HA RM. Analyzed the data: TK YH TT NS. Contributed reagents/materials/analysis tools: TK TM TA MM TS. Wrote the paper: TK YH TT NS.

References

1. Cho KR, Shih Ie M (2009) Ovarian cancer. Annu Rev Pathol 4: 287–313.
2. Perren TJ, Swart AM, Pfisterer J, Ledermann JA, Pujade-Lauraine E, et al. (2011) A phase 3 trial of bevacizumab in ovarian cancer. N Engl J Med 365: 2484–2496.
3. Goff B (2012) Symptoms associated with ovarian cancer. Clin Obstet Gynecol 55: 36–42.
4. Bast RC Jr, Hennessy B, Mills GB (2009) The biology of ovarian cancer: new opportunities for translation. Nat Rev Cancer 9: 415–428.
5. Parmar MK, Ledermann JA, Colombo N, du Bois A, Delaloye JF, et al. (2003) Paclitaxel plus platinum-based chemotherapy versus conventional platinum-based chemotherapy in women with relapsed ovarian cancer: the ICON4/AGO-OVAR-2.2 trial. Lancet 361: 2099–2106.
6. Ledermann J, Harter P, Gourley C, Friedlander M, Vergote I, et al. (2012) Olaparib maintenance therapy in platinum-sensitive relapsed ovarian cancer. N Engl J Med 366: 1382–1392.
7. Reya T, Morrison SJ, Clarke MF, Weissman IL (2001) Stem cells, cancer, and cancer stem cells. Nature 414: 105–111.
8. Visvader JE, Lindeman GJ (2008) Cancer stem cells in solid tumours: accumulating evidence and unresolved questions. Nat Rev Cancer 8: 755–768.
9. Hirohashi Y, Torigoe T, Inoda S, Morita R, Kochin V, et al. (2012) Cytotoxic T lymphocytes: Sniping cancer stem cells. Oncoimmunology 1: 123–125.
10. Dean M, Fojo T, Bates S (2005) Tumour stem cells and drug resistance. Nat Rev Cancer 5: 275–284.
11. Rich JN (2007) Cancer stem cells in radiation resistance. Cancer Res 67: 8980–8984.
12. Hirohashi Y, Torigoe T, Inoda S, Takahashi A, Morita R, et al. (2010) Immune response against tumor antigens expressed on human cancer stem-like cells/tumor-initiating cells. Immunotherapy 2: 201–211.
13. Al-Hajj M, Wicha MS, Benito-Hernandez A, Morrison SJ, Clarke MF (2003) Prospective identification of tumorigenic breast cancer cells. Proc Natl Acad Sci U S A 100: 3983–3988.
14. Singh SK, Hawkins C, Clarke ID, Squire JA, Bayani J, et al. (2004) Identification of human brain tumour initiating cells. Nature 432: 396–401.
15. Zhang S, Balch C, Chan MW, Lai HC, Matei D, et al. (2008) Identification and characterization of ovarian cancer-initiating cells from primary human tumors. Cancer Res 68: 4311–4320.
16. Zhang WC, Shyh-Chang N, Yang H, Rai A, Umashankar S, et al. (2012) Glycine decarboxylase activity drives non-small cell lung cancer tumor-initiating cells and tumorigenesis. Cell 148: 259–272.
17. Goodell MA, Brose K, Paradis G, Conner AS, Mulligan RC (1996) Isolation and functional properties of murine hematopoietic stem cells that are replicating in vivo. J Exp Med 183: 1797–1806.
18. Nakatsugawa M, Takahashi A, Hirohashi Y, Torigoe T, Inoda S, et al. (2011) SOX2 is overexpressed in stem-like cells of human lung adenocarcinoma and augments the tumorigenicity. Lab Invest 91: 1796–1804.
19. Gangavarpu KJ, Huss WJ (2011) Isolation and applications of prostate side population cells based on dye cycle violet efflux. Curr Protoc Toxicol Chapter 22: Unit 22 22.
20. Ginestier C, Hur MH, Charafe-Jauffret E, Monville F, Dutcher J, et al. (2007) ALDH1 is a marker of normal and malignant human mammary stem cells and a predictor of poor clinical outcome. Cell Stem Cell 1: 555–567.
21. Huang EH, Hynes MJ, Zhang T, Ginestier C, Dontu G, et al. (2009) Aldehyde dehydrogenase 1 is a marker for normal and malignant human colonic stem cells (SC) and tracks SC overpopulation during colon tumorigenesis. Cancer Res 69: 3382–3389.
22. Nishida S, Hirohashi Y, Torigoe T, Kitamura H, Takahashi A, et al. (2012) Gene expression profiles of prostate cancer stem cells isolated by aldehyde dehydrogenase activity assay. J Urol 188: 294–299.
23. Deng S, Yang X, Lassus H, Liang S, Kaur S, et al. (2010) Distinct expression levels and patterns of stem cell marker, aldehyde dehydrogenase isoform 1 (ALDH1), in human epithelial cancers. PLoS One 5: e10277.
24. Silva IA, Bai S, McLean K, Yang K, Griffith K, et al. (2011) Aldehyde dehydrogenase in combination with CD133 defines angiogenic ovarian cancer stem cells that portend poor patient survival. Cancer Res 71: 3991–4001.
25. Wang YC, Yo YT, Lee HY, Liao YP, Chao TK, et al. (2012) ALDH1-bright epithelial ovarian cancer cells are associated with CD44 expression, drug resistance, and poor clinical outcome. Am J Pathol 180: 1159–1169.
26. Chang B, Liu G, Xue F, Rosen DG, Xiao L, et al. (2009) ALDH1 expression correlates with favorable prognosis in ovarian cancers. Mod Pathol 22: 817–823.
27. Yabushita H, Ueno N, Sawaguchi K, Higuchi K, Noguchi M, et al. (1989) Establishment and characterization of a new human cell-line (AMOC-2) derived from a serous adenocarcinoma of ovary. Nihon Sanka Fujinka Gakkai Zasshi 41: 888–894.
28. Ishiwata I, Ishiwata C, Kobayashi N, Ishikawa H (1987) Characterization of newly established cell line HUOA from a human ovarian serous cystadenocarcinoma. Nihon Sanka Fujinka Gakkai Zasshi 39: 831–836.
29. Kobayashi S, Yamada-Okabe H, Suzuki M, Natori O, Kato A, et al. (2012) LGR5-Positive Colon Cancer Stem Cells Interconvert with Drug Resistant LGR5-Negative Cells and are Capable of Tumor Reconstitution. Stem Cells.
30. Kitamura H, Torigoe T, Hirohashi Y, Asanuma H, Inoue R, et al. (2012) Prognostic impact of the expression of ALDH1 and SOX2 in urothelial cancer of the upper urinary tract. Mod Pathol.
31. Michifuri Y, Hirohashi Y, Torigoe T, Miyazaki A, Kobayashi J, et al. (2012) High expression of ALDH1 and SOX2 diffuse staining pattern of oral squamous cell carcinomas correlates to lymph node metastasis. Pathol Int 62: 684–689.
32. Szotek PP, Pieretti-Vanmarcke R, Masiakos PT, Dinulescu DM, Connolly D, et al. (2006) Ovarian cancer side population defines cells with stem cell-like characteristics and Mullerian Inhibiting Substance responsiveness. Proc Natl Acad Sci U S A 103: 11154–11159.
33. Vathipadiekal V, Saxena D, Mok SC, Hauschka PV, Ozbun L, et al. (2012) Identification of a potential ovarian cancer stem cell gene expression profile from advanced stage papillary serous ovarian cancer. PLoS One 7: e29079.
34. Curley MD, Therrien VA, Cummings CL, Sergent PA, Koulouris CR, et al. (2009) CD133 expression defines a tumor initiating cell population in primary human ovarian cancer. Stem Cells 27: 2875–2883.
35. Shi MF, Jiao J, Lu WG, Ye F, Ma D, et al. (2010) Identification of cancer stem cell-like cells from human epithelial ovarian carcinoma cell line. Cell Mol Life Sci 67: 3915–3925.
36. Gao MQ, Choi YP, Kang S, Youn JH, Cho NH (2010) CD24+ cells from hierarchically organized ovarian cancer are enriched in cancer stem cells. Oncogene 29: 2672–2680.
37. Shmelkov SV, Butler JM, Hooper AT, Hormigo A, Kushner J, et al. (2008) CD133 expression is not restricted to stem cells, and both CD133+ and CD133- metastatic colon cancer cells initiate tumors. J Clin Invest 118: 2111–2120.
38. Burkert J, Otto WR, Wright NA (2008) Side populations of gastrointestinal cancers are not enriched in stem cells. J Pathol 214: 564–573.
39. Chan JK, Teoh D, Hu JM, Shin JY, Osann K, et al. (2008) Do clear cell ovarian carcinomas have poorer prognosis compared to other epithelial cell types? A study of 1411 clear cell ovarian cancers. Gynecol Oncol 109: 370–376.
40. Miyamoto M, Takano M, Goto T, Kato M, Sasaki N, et al. (2013) Clear cell histology as a poor prognostic factor for advanced epithelial ovarian cancer: a single institutional case series through central pathologic review. J Gynecol Oncol 24: 37–43.

EXPERIMENTAL CELL RESEARCH 319 (2013) 2617–2626

Available online at www.sciencedirect.com

ScienceDirect

journal homepage: www.elsevier.com/locate/yexcr

Research Article

Six-transmembrane epithelial antigen of the prostate-1 plays a role for in vivo tumor growth via intercellular communication

Takashi Yamamoto[a,b], *Yasuaki Tamura*[a,*], *Jun-ichi Kobayashi*[b], *Kenjirou Kamiguchi*[a], *Yoshihiko Hirohashi*[a], *Akihiro Miyazaki*[b], *Toshihiko Torigoe*[a], *Hiroko Asanuma*[c], *Hiroyoshi Hiratsuka*[b], *Noriyuki Sato*[a]

[a]*Department of Pathology, Sapporo Medical University School of Medicine, South 1, West 17, Chuo-ku, Sapporo 060-8556, Japan*
[b]*Department of Oral Surgery, Sapporo Medical University School of Medicine, Sapporo, Japan*
[c]*Department of Clinical Pathology, Sapporo Medical University School of Medicine, Sapporo, Japan*

ARTICLE INFORMATION

Article Chronology:
Received 16 February 2013
Received in revised form
5 July 2013
Accepted 26 July 2013
Available online 2 August 2013

Keywords:
STEAP-1
Intercellular communication
Tumor stromal cell
miRNA

ABSTRACT

Six-transmembrane epithelial antigen of the prostate-1 (STEAP-1) is a novel cell surface protein overexpressed only in the prostate among normal tissues and various types of cancer including prostate, bladder, lung, and ovarian cancer. Although its function in prostate and tumor cells has been remained unclear, due to its unique and restricted expression, STEAP-1 is expected to be an attractive target for cancer therapy. Here, we show that knockdown of STEAP-1 in human cancer cells caused the retardation of tumor growth compared with wild type in vivo. In contrast, STEAP-1 introduced tumor cells augmented the tumor growth compared with STEAP-1-negative wild type cells. Using dye transfer assay, we demonstrate that the STEAP-1 is involved in intercellular communication between tumor cells and adjacent tumor stromal cells and therefore may play a key role for the tumor growth in vivo. These data indicate the inhibition of the STEAP-1 function or expression can be a new strategy for cancer therapy.

Introduction

The six-transmembrane epithelial antigen of the prostate-1 (STEAP-1) is an attractive target for gene therapy because it is overexpressed only in the prostate among normal tissues and various types of cancer including prostate, bladder, lung, and ovarian cancer [1]. Due to its unique and restricted expression, STEAP-1-derived peptide has been demonstrated to be a promising cancer antigen for immunotherapy [2–5]. In addition, structure analysis suggested that STEAP-1 might act as a channel, receptor, or transporter protein [6]. However, it has been unclear for its function in prostate as well as tumor cells. A cell's ability to effectively communicate with a neighboring cell is essential for tissue function and the maintenance for homeostasis. One important mode of intercellular communication is the release of soluble cyto- and chemokines. Once secreted, these signaling molecules diffuse through the surrounding medium and eventually bind to neighboring cell's receptors whereby the signal is received. This mode of communication is governed both by physiochemical transport processes and cellular secretion rates, which in turn are determined by genetic and

*Corresponding author. Fax: +81 11 643 2310.
E-mail addresses: ytamura@sapmed.ac.jp, ytamura3566@gmail.com (Y. Tamura).

0014-4827/$ - see front matter © 2013 Elsevier Inc. All rights reserved.
http://dx.doi.org/10.1016/j.yexcr.2013.07.025

biochemical processes. It has been demonstrated that gap junction channels, composed of connexin (Cx), mediate reciprocal exchange of ions and small molecules of less than 1000 Da, including second messenger cyclic AMP, IP3, and Ca^{2+}, between adjacent cells [7]. Such gap junctional intercellular communication plays a fundamental function in the regulation of cell and tissue homeostasis. However, it has been reported that Cx gene transcription and the protein expression decreased along with the development of the cancer [7–9]. Moreover, the trafficking and localization of Cx is frequently deregulated in cancer cells. In fact, it has been demonstrated that *Cx-43* mRNA is downregulated in PC3, LNCaP, and DU145 prostate carcinoma cells in comparison to normal prostate epithelial cells [10,11]. Thus, Cxs have been considered to act as tumor suppressor genes. Recently, it has been emphasized that the formation and progression of tumor mass requires communication between cancer cells and adjacent stromal cells, to regulate patterns of growth and differentiation. These facts suggest that the mechanisms other than the Cx-mediated intercellular communication may exist. Moreover, it has been demonstrated that adjacent stromal cells fueled cancer cells to invade and metastasize. These facts suggested that instead of Cx family members, some sort of transporter or channel molecules responsible for the tumor growth must exist. More importantly, the disruption or modification in this process might lead to tumor dormant state and can be a new strategy for cancer therapy. Recently, Challita-Eid et al. has demonstrated that STEAP-1 acted as a channel molecule for intercellular communication of small molecules [6]. They have shown that blocking of STEAP-1 expressed on tumor cells using mAb against STEAP-1 in vivo resulted in the loss of intercellular communication of small molecules, leading to antitumor effect. However, it has been still unclear that what kinds of small molecules are transported through STEAP-1, which is required for tumor growth in vivo. In addition, it should be clear whether STEAP-1 plays a role in intercellular communication between cancer cells and cancer-associated stromal cells such as fibroblasts, endothelial cells, and macrophages. Therefore, we examined the role of STEAP-1 involved in tumor development using miRNA-based silencing or overexpression of STEAP-1 molecules. We used intercellular dye transfer methods to assess the intercellular communication between cancer cells and cancer-associated stromal cells, and showed that knockdown of STEAP-1 in human cancer cells impaired the intercellular communication. Importantly, we found that not only cancer cells but also cancer-associated stromal cell expressed STEAP-1 although its expression level was limited. Furthermore, our study showed that STEAP-1 is involved in intercellular communication between the cancer cells and adjacent cancer stromal cells and the expression of STEAP-1 might be essential for tumor mass development.

Materials and methods

Cell lines and culture media

Human oral squamous cell carcinoma cell lines, OSC20, OSC30 were established in our laboratory. Human prostate cancer cell lines, DU145 and LNCaP was purchased from ATCC. Methylchoranthrene-induced murine fibrosarcoma cell line TG3 was established in our laboratory [12]. These cells were cultured in RPMI 1640 (Sigma-Aldrich, St. Louis, MO) medium supplemented with 2 mM L-glutamine, 10% fetal bovine serum, 100 U/ml penicillin G, and 100 μg/ml streptomycin at 37 °C in a humidified 5% CO_2 atmosphere.

RT-PCR analysis

Total RNA was isolated from cultured cells by using ISOGEN reagent (Nippon Gene, Tokyo, Japan). The cDNA mixture was synthesized from 1 μg of total RNA by reverse transcription using Superscript III and oligo (dT) primer (Life Technologies, Inc., Gaithersburg, MD) according to the manufacturer's protocol. PCR amplification was performed in 50 μl of PCR mixture containing 1 μL of the cDNA mixture, KOD Plus DNA polymerase (Toyobo, Osaka, Japan), and 50 pmol of primers. The PCR mixture was initially incubated at 92 °C for 2 min, followed by 30 cycles of denaturation at 92 °C for 1 min, annealing at 62 °C for 1 min, and extension at 72 °C for 1 min. Primer pairs used for RT-PCR analysis were 5′-ACTTTGTTGATGACCAGGATTGG-3′ and 5′-CAGAACTTCAG-CACACACAGGAA-3′ for human *STEAP-1*, 5′-GGTGGCTGAAGCCG-TACTAT-3′ and 5′-GGATGATATGATGGCAGCGAC-3′ for murine *STEAP-1* as a forward and a reverse primer, respectively. Human *Cx-43* was detected by using a forward primer 5′-GGGTTAAGG-GAAAGAGCGACC-3′ and a reverse primer 5′-CCCCATTC-GATTTTGTTCTGC-3′. Human *Cx32* was detected by using a forward primer 5′-ATGAACTGGACAGGTTTGTACACCTTGCTC-3′ and a reverse primer 5′-TCAGCAGGCCGAGCAGCGG-3′. As an internal control *glyceraldehyde-3-phosphate dehydrogenase* (*G3PDH*) was detected by using a forward primer 5′-ACCACAGTC-CATGCCATCAC-3′ and a reverse primer 5′-TCCACCACCC-TGTTGCTGTA-3′. Murine *G3PDH* was detected by using a forward primer 5′-CTGAACGGGAAGCTCACTG-3′ and a reverse primer 5′-TGAGGTCCACCACCCTGTTG-3′. The PCR products were visualized with ethidium bromide staining under UV light after electrophoresis on 1.0% agarose gel. Nucleotide sequence of the PCR products was confirmed by direct sequencing using ABI Genetic analyzer PRISM 310 and an AmpliCycle sequencing kit (Perkin-Elmer, Foster City, CA).

Western blotting

Cultured cells were washed in ice-cold PBS, lysed by incubation on ice in a lysis buffer [50 mmol/L Tris–HCl (pH 8.0), 150 mmol/L NaCl, 1% NP40, protease inhibitor cocktail; complete (Roche Diagnostics, Inc., Basel, Switzerland)], and cleared by centrifugation at 15,000 rpm for 20 min at 4 °C. The whole-cell lysates were boiled for 5 min in the presence of SDS sample buffer, resolved by 10% SDS-PAGE, and electrophoretically transferred to polyvinylidene difluoride (PVDF) membranes (Immobilon-P, Millipore, Billerica, MA). The membranes were then incubated with blocking buffer (5% nonfat dry milk in PBS) for 1 h at room temperature and then incubated for 60 min with rabbit anti-STEAP polyclonal antibody (Zymed laboratories Inc), anti-human Cx43 mAb (Zymed laboratories Inc), or mouse anti-β-actin monoclonal antibody AC-15 (Sigma-Aldrich). After washing three times with wash buffer (0.1% Tween-20 in PBS), the membrane was reacted with peroxidase-labeled goat anti-rabbit IgG antibody (KPL, Gaithersburg, MD) for 2 h. Finally, the signal was visualized by using an enhanced chemiluminescence (ECL) detection system (Amersham Life Science, Arlington Heights, IL) according to the manufacturer's protocol.

Proliferation assay

The cell proliferation assays based on the cleavage of the tetrazolium salt WST-1 (DOJINDO) by mitochondrial dehydrogenases in viable cells was performed according to the manufacturer's instruction. The cells were seeded on 96-well microtiter tissue culture plates in the 10% serum at the density of 1×10^3 cells/well. After incubation at 37 °C for 24–72 h, WST-1 reagent (10 μL) was added to the cells and incubated at 37 °C in 96-well microtiter tissue culture plates for 2 h at 37 °C. The amount of produced formazan dye, which directly correlates to the number of metabolically active cells in culture, was quantified by measuring the absorbance at wavelength of 450 nm, using a microtiter plate (ELISA) reader.

Plasmid construction and transfection

A human *STEAP-1* cDNA was ligated into the BamHI and EcoRI sites of the *pcDNA3.1* mammalian expression vector (Invitrogen). The clones from STEAP-1-overexpressed OSC30 were established using 1 mg/ml of G418 selection (Life Technologies). The expression of STEAP-1 was confirmed by western blotting using pAb against STEAP (Zymed). Primers for microRNAs (miRNAs) against *STEAP-1* were selected using the BLOCK-iT™ RNAi Designer (Invitrogen). The oligonucleotide sequence was as follows: 5′-AGCAGCAATTGTCCAACTTCA-3′ (405), 5′-TGAGGCGATCCTACAGATACA-3′ (551), 5′-ATGATGTTTGGAGAATGGAGA-3′ (632), 5′-GACTCTTTGACATGGAGAGAA-3′ (727), 5′-GTCAAGCTGGCGAAGAGTG-3′ (53). To knockdown STEAP-1 expression by RNA interference, doublestranded oligonucleotides targeting the human *STEAP-1* gene and a negative control sequence derived from the MISSION nontarget miRNA control vector were ligated into the pcDNA™6.2-GW/miR vector (Invitrogen) according to the manufacturer's instructions. Following sequencing of individual clones, the ability of each of the five *STEAP-1* miRNA constructs to suppress *STEAP-1* mRNA levels was measured by RT-PCR. Briefly, each cell line at 80% confluency was transfected with the *STEAP-1* miRNA vectors using Lipofectamine 2000 Reagent (Invitrogen, Carlsbad, CA) according to the manufacturer's instructions. For establishing the stable clone, 10 μg/ml of blasticidin (Sigma-Aldrich, St. Louis, MO) was added to the culture 48 h after transfection.

In vivo studies

To demonstrate the relationship between STEAP-1 expression and tumorigenicity while excluding immunogenicity of tumors, we challenged immunocompromised NOD/SCID mice with tumor cells and compared tumor growth. Female NOD/SCID mice, 5–6 weeks old, were obtained from the Jackson Laboratory (Bar Harbor, ME, USA) and used at 6 weeks of age. Mice were maintained in a specific pathogen-free mouse facility at Sapporo Medical University according to institutional guidelines for animal use and care. For tumor formation studies, mice were injected s.c. with 1×10^6 DU145 or OSC30 cells. Tumor length and width were measured with a caliper. Tumor volumes were calculated using the following formula: length × width^2 × 0.5. All the experiments were performed with 5 mice/group. Average tumor volumes on day 35 or 37 were statistically analyzed using the Mann–Whitney U test.

Intercellular communication assay

Intercellular communication was measured using a fluorescent dye transfer assay adapted from previously published studies [6]. Briefly, accepter cells were preloaded with the dye dextran-Texas red (10 kDa; 1 mg/ml, Invitrogen/Molecular Probes) overnight at 37 °C through endocytosis. Donor cells were preloaded with 5 μg/mL of the green dye calcein AM (1 kDa; Invitrogen/Molecular Probes) for 1 h at 37 °C. Donor cells were layered over acceptor cells at a ratio of 1:3. Cells were incubated at 37 °C for 6 h. Percentage transfer was calculated as the fraction of cells that accepted the green dye (yellow/orange cells) in the total population of acceptor cells (yellow/orange and red cells). Transfer was measured by counting the number of cells in five different fields using fluorescence microscopy.

Inhibition of gap junction activity

Inhibitors of gap junctional communication, carbenoxolone, a synthetic derivative of glycyrrhetinic acid (CBX, Sigma-Aldrich) [13] and doxyl stearic acids (DSA, Sigma-Aldrich) [14] was examined as to their effects on intercellular communication of STEAP-1-expressing cells. Donor cells were first loaded with calcein AM. After extensive washing, the cells were treated with HEPES buffer containing 150 μM CBX or 50 μM DSA. After 10 min, the cells were layered over acceptor cells loaded with dextran–Texas red at a ratio of 1:3. Cells were incubated at 37 °C for 3 h. Percentage transfer was calculated as the fraction of cells that accepted the green dye (yellow/orange cells) in the total population of acceptor cells (yellow/orange and red cells).

Isolation of stromal cells

Mice were injected s.c. with 1×10^6 DU145 cells. Mice were sacrificed when tumor diameter reached ~20 mm and excised the tumors. Thereafter, they were cultured in AIM-V medium (Life Technologies) containing 0.05% collagenase Type I (Sigma-Aldrich) overnight at 4 °C. Stromal cells were then isolated by negative selection using anti-CD326 (EpCAM) monoclonal antibody coupled with magnetic microbeads and the MACS separation system (Miltenyi Boitech, Bergish Blabach, Germany) according to the manufacturer's instruction. Flow cytometric analysis was performed to detect murine H-2 K^d using mAb SF1-1.1 (BD Biosciences) and murine CD11b using mAb clone M1/70 (BD Biosciences).

Histopathological study of tumor sections

NOD/SCID mice were injected s.c. with 1×10^6 DU145 cells or DU145-miRNA cells. Mice were sacrificed when tumor diameter reached ~10 mm and excised the tumors and fixed in 10% formalin in PBS. Paraffin-embedded sections were then prepared and processed for hematoxylin–eosin (HE)-staining. For immunohistochemical analysis, sections were stained with anti-human Cx43 mAb (Zymed laboratories Inc) and then incubated with HRP-conjugated goat anti-mouse Ig (Dako), followed by hematoxylin counterstaining.

Statistical analysis

Results were given as means±SE. Comparison between two groups was made by Student's *t* tests (two-tailed) for grouped data. For xenograft studies, mean tumor diameter among groups were compared using the Mann–Whitney U test. Significance in all tests was set at 95% or greater confidence level.

Results

Cell line generation

We established the cell lines, which were knocked-down the expression of STEAP-1 using miRNA for RNA interference. STEAP-1 positive prostate cancer cell line DU145 and human oral squamous cell carcinoma line OSC20 were transfected with miRNA RNAi expression vectors targeting *STEAP-1* gene and generated STEAP-1-knockdown cell clones. As shown in Fig. 1A and B, both DU145-miRNA clone and OSC20-miRNA clone showed a significant decrease of STEAP-1 expression by RT-PCR and Western blotting. Prostate cancer cell line LNCaP served as a positive control. Western blot analysis indicated that the loss of STEAP-1 protein in these cells was maintained for more than 60 days. Furthermore, we established the cell clones, of which were transfected with *STEAP-1* cDNA to overexpress STEAP-1. Human oral squamous cell carcinoma line OSC30 did not express STEAP-1 at protein level (Fig. 1C). Therefore, STEAP-1 negative OSC30 was transfected with *STEAP-1* cDNA. The stable clones showed increase of the expression of STEAP-1 (Fig. 1C).

Expression of STEAP-1 does not correlate to the proliferation of cancer cell lines in vitro

To determine whether the expression of STEAP-1 could affect the cell proliferation of cell lines in vitro, proliferative responses were measured using WST-1 assay. In cell proliferation of DU145 cell, no differences were observed when compared with DU145-miRNA cell and mock control cell (Fig. 2A). Similarly, there were no differences between OSC20 cell and OSC20-miRNA cell and mock control cell (Fig. 2B). Furthermore, we did not observe the statistical significance between STEAP-1-negative OSC30 cell and STEAP-1-introduced OSC30 cell (Fig. 2C). These data indicated that the expression of STEAP-1 did not affect the cell proliferation of cell lines in vitro.

Effect of STEAP-1 expression on tumor growth in vivo

We performed xenograft experiments to determine the impact of STEAP-1 on in vivo tumor growth in immunocompromised NOD/SCID mice. To investigate the effect of STEAP-1 knockdown on tumor growth in vivo, these mice were injected s.c. with 1×10^6 DU145, DU145-mock or DU145-miRNA. Fig. 3A shows that tumor volume of the DU145-miRNA cell line is significantly smaller than that of DU145 parental line and DU145 mock ($P<0.01$). Furthermore, STEAP-1-negative OSC30 and STEAP-1-introduced OSC30-STEAP-1 tumor cells were compared for tumor growth. Results showed that tumor volume of the OSC30-STEAP-1 cell line was greater than that of the OSC30 parental cell line ($P<0.05$) (Fig. 3B). These results clearly demonstrated that expression of STEAP-1 accelerated growth rate in vivo, indicating a critical role of STEAP-1 in the regulation of cell growth in vivo.

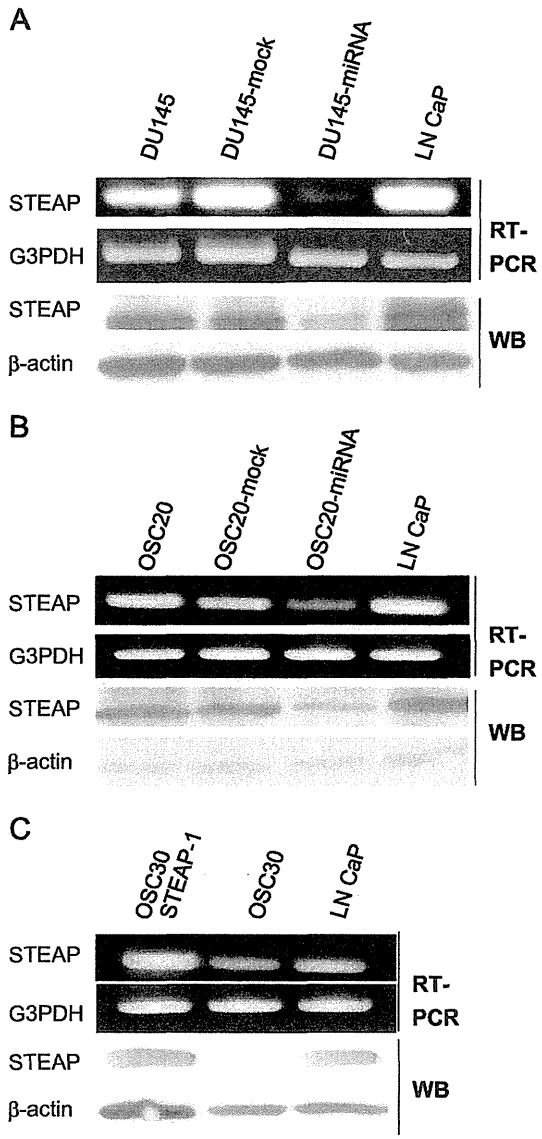

Fig. 1 – Cell line generation. (A) RT-PCR and Western blot analysis demonstrate that DU145 cells expressing a *STEAP-1* miRNA have dramatically reduced mRNA and protein levels in comparison to DU145 cells and DU145 mock control cells. (B) OSC20 cells expressing a *STEAP-1* miRNA have reduced mRNA and protein levels in comparison to OSC20 cells and OSC20 mock control cells. (C) RT-PCR and Western blot analysis demonstrated OSC30 cells transfected with a *STEAP-1* cDNA have increased mRNA and protein levels of STEAP-1. The prostatic cancer cell line LNCaP cell serves as a positive control.

STEAP-1 is required for intercellular communication activity

Challita-Eid et al. have shown that blocking STEAP-1 using mAb against STEAP-1 inhibited intercellular communication in vitro

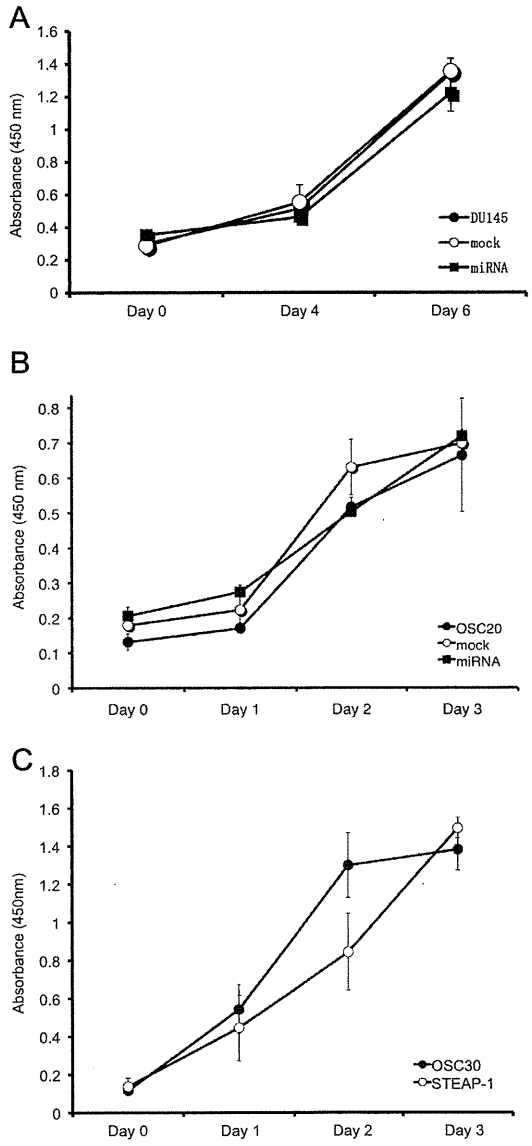

Fig. 2 – Expression of STEAP-1 does not correlate to the proliferation of cell lines in vitro. The cells were seeded on 96-well microtiter tissue culture plates in the 10% serum at the density of 1×10^3 cells/well. After incubation at 37 °C for 24–72 h, WST-1 assay was carried out. (A) In DU145 cells or (B) in OSC20 cells, the expression of STEAP-1 did not affect the proliferation of cell lines in vitro. (C) In OSC30 cells, overexpression of STEAP-1 did not affect the proliferation of cell lines in vitro. Each point represents the mean and SD of O. D in triplicate wells. Data are representative of three independent experiments. In any experiments, statistical analysis using Student's *t* tests (two-tailed) does not show the statistical significance.

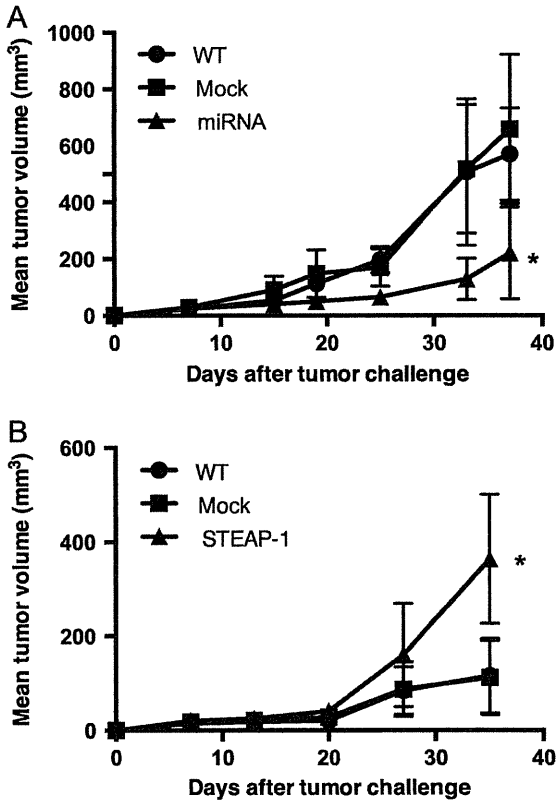

Fig. 3 – The expression of STEAP-1 significantly affects the tumor growth in vivo. (A) DU145, DU145-mock, and DU145-miRNA cells were injected s.c. into NOD/SCID mice ($n=5$). Tumor size was measured at the indicated time points. Each point represents the mean and SD of tumor volume. Statistical analysis using the Mann–Whitney U test for average tumor volumes on day 37 shows $P<0.01$ for DU145-miRNA cells compared with DU145, DU145-mock cells. Data are representative of three independent experiments. (B) OSC 30, OSC30-mock, OSC30-STEAP-1 cells were injected s. c into NOD/SCID mice ($n=5$). Tumor size was measured at the indicated time points. Each point represents the mean and SD of tumor volume. Statistical analysis using the Mann–Whitney U test for average tumor volumes on day 35 shows $P<0.05$ for OSC30 or OSC30-mock cells compared with OSC30-STEAP-1 cells. Data are representative of three independent experiments.

and in vivo [6]. To confirm the STEAP-1 function as a transporter of small molecules (<1 kDa) between cells, we performed the dye transfer assay using a fluorescent (see Materials and methods). DU145 and OSC20, which does express STEAP-1 and OSC30, which does not express STEAP-1 were chosen for the assay. Donor cells loaded with calcein AM and acceptor cells loaded with dextran–Texas red were mixed. Dye transfer, as manifested by intracellular yellow/orange fluorescence, was not detected between donor and acceptor cells that did not express STEAP-1 nor between cells in which only one partner expressed STEAP-1. In brief, the transfer of the material from DU145 to DU145 was observed, however the transfer of it from DU145-miRNA to DU145 was not observed (Fig. 4A). Similarly, the transfer of the material from OSC20 to OSC20 was observed, however the transfer of it from OSC20-miRNA to OSC20 was not observed (Fig. 4B). Furthermore, the transfer of the material from OSC30-STEAP-1 to OSC30-STEAP-1 was observed, however the transfer of it from OSC

30-STEAP-1 to OSC30, from OSC 30 to OSC30-STEAP-1 and from OSC30 to OSC30 was not observed (Fig. 4C). In conclusion, extensive dye transfer was observed in almost all cells in cultures where both donor and acceptor cells expressed STEAP-1 (Fig. 4D). In contrast, dye transfer was not detected between cells in which only one partner expressed STEAP-1. These results suggested the STEAP-1 played a very important role for intercellular communication for small molecules between the cells.

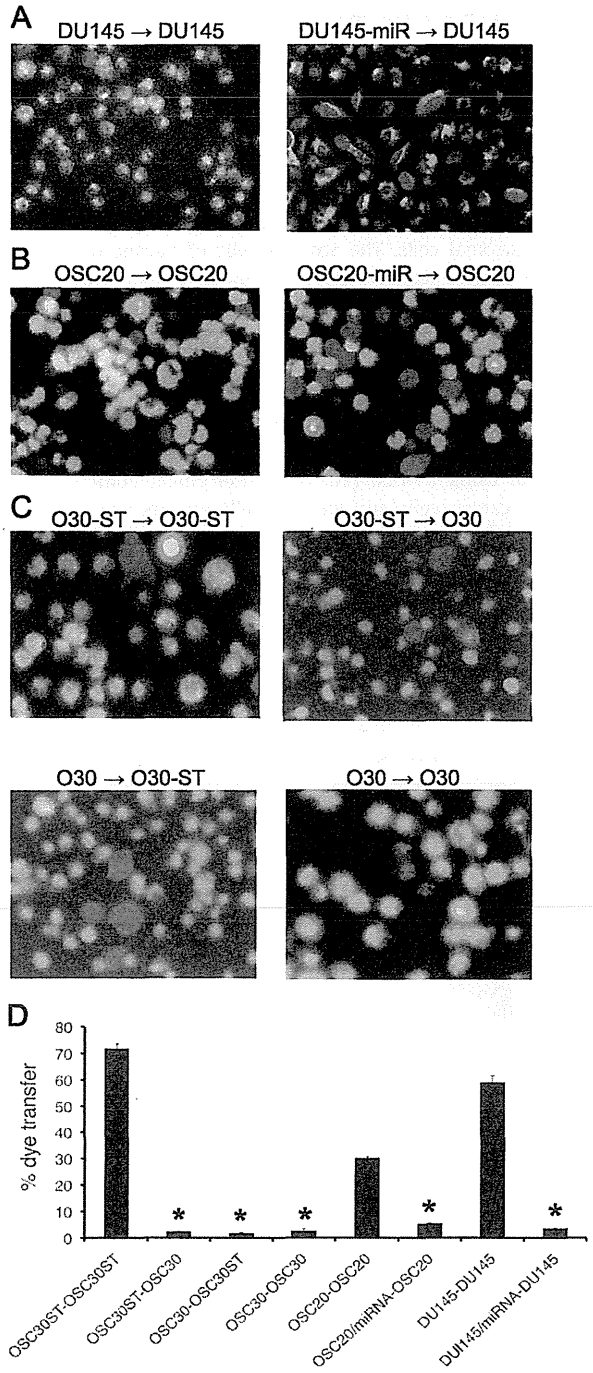

Fig. 4 – STEAP-1 plays a role in intercellular communication in various types of tumor cells. Donor and acceptor cells were loaded with calcein AM (donor) or dextran–Texas red (acceptor) dyes and mixed 1:3 to allow intercellular communication to occur as manifested by the appearance of the yellow/orange color (see Materials and methods). (A) Representative pictures were taken from DU145–DU145, DU145-miRNA–DU145 populations. (B) Representative pictures were taken from OSC20–OSC20, OSC20-miRNA–OSC20 populations. (C) Representative pictures were taken from OSC30-STEAP-1–OSC30-STEAP-1, OSC30-STEAP-1–OSC30, OSC30–OSC30-STEAP-1, OSC30–OSC30 populations. (D) Percentage transfer was calculated as the fraction of cells that accepted the green dye (yellow/orange cells) in the total population of acceptor cells (yellow/orange and red cells). Transfer was measured by counting the number of cells in five different fields using fluorescence microscopy. Statistical analysis using Student's *t* tests (two-tailed) for percentage dye transfer shows $P<0.01$ for OSC30-STEAP-1–OSC30-STEAP-1 compared with OSC30-STEAP-1–OSC30, OSC30–OSC30-STEAP-1 and OSC30–OSC30 populations, $P<0.01$ for OSC20–OSC20 compared with OSC20-miRNA–OSC20 populations, $P<0.01$ for DU145–DU145 compared with DU145-miRNA–DU145 populations. Data are representative of three independent experiments.

Cx43 appears uninvolved in the intercellular communication in DU145 cells

With respect to intercellular communication, Cx family proteins including Cx43 and Cx32 have been demonstrated to play a central role [11]. Among Cx family members, it has been reported that Cx43 gene transcription and protein expression decreased with development of the cancer [11,15]. In contrast, forced expression of both Cx43 and Cx32 genes in Cx-deficient LNCaP cells inhibited tumor growth, suggesting that a loss of the appropriate assembly of Cx43 and Cx32 into gap junctions results in the development of prostate cancer [9]. Therefore, we compared expression levels of the representative genes Cx43 and Cx32 in DU145 and DU145-miR cells. RT-PCR and Western blotting revealed that Cx43 was expressed in DU145 and DU145-miR cells at similar levels (Fig. 5A and B). On the other hand, immunohistochemical analysis revealed that Cx43 was mainly localized within the cytoplasm but not at the cell surface of DU145 cells (Fig. 5C) and DU145-miR cells (data not shown), suggesting that Cx43 is not able to form a gap junctional channel. In contrast, we did not detect expression of Cx32 at the mRNA level. These results indicated that Cx43 and Cx32 were not involved in the intercellular communication. Moreover, we examined whether gap junction inhibitors carbenoxolone (CBX) and doxyl stearic acids (DSA) affected the intercellular communication. We observed that the treatment of DU145 cells (Fig. 6A) or OSC30-STEAP-1 cells (Fig. 6B) with CBX and DSA did not inhibit the intercellular communication, rather somewhat augmented. These results may suggest that inhibition of gap junctional communication shifted in intercellular communication to the STEAP-1-mediated communication. Collectively, our results suggested that STEAP-1, but not Cx43 or Cx32, played a pivotal role at

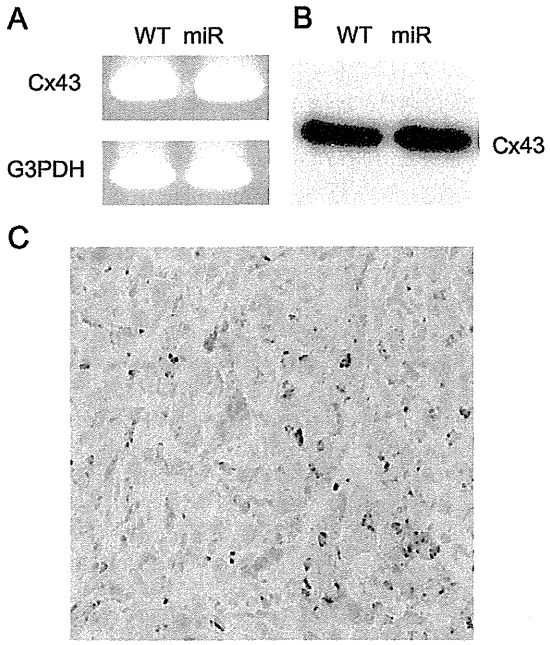

Fig. 5 – Cx43 expression in DU145 and DU145-miRNA cells. (A) RT-PCR and (B) Western blot analysis demonstrates the mRNA and protein level of Cx43 in DU145 and DU145-miRNA cells. (C) Immunohistochemical analysis of Cx43 in DU145 cells. NOD/SCID mice were injected s.c. with 1×10^6 DU145 cells. Mice were sacrificed when tumor diameter reached ~10 mm and excised the tumors and fixed in 10% formalin in PBS. For immunohistochemical analysis, sections were stained with anti-human Cx43 mAb (x200).

least in part in the intercellular communication for tumor growth in DU145 cells. Moreover, considering the results from the differences between in vitro tumor cell proliferation assay and in vivo tumor growth, STEAP-1 might be important for cell–cell interaction between tumor cells and surrounding stromal cells, but not tumor cells and tumor cells. Therefore, we asked whether the STEAP-1 involved the intercellular communication between tumor-associated stromal cells and tumor cells.

STEAP-1 plays an important role in intercellular communication between cancer cells and cancer-associated stromal cells

It has been well demonstrated that tumor growth in vivo requires the interaction between tumor cells and adjacent stromal cells, such as macrophages, endothelials and fibroblasts. To evaluate the impact of STEAP-1 expression on the intercellular communication between tumor cells and cancer-associated stromal cells, we performed the intercellular communication assay using cancer-derived stromal cells. The stromal cells of murine origin were isolated from established DU145 tumor mass by negative selection using anti-human CD326 (EpCAM) microbeads and MACS separation system. They were confirmed to be the murine origin because of carrying murine MHC class I molecules ($H\text{-}2^d$) by flow cytometry (Fig. 7A) and were included fibroblasts and $CD11b^+$ macrophages (data not shown). Furthermore, we confirmed that the isolated murine stromal cells expressed murine *STEAP-1* at low level using RT-PCR (Fig. 7B). Intercellular communication between cancer cells and stromal cells was measured using a fluorescent dye transfer assay. The DU145, which does express STEAP-1 was chosen for the assay. DU145 or DU145-miRNA as

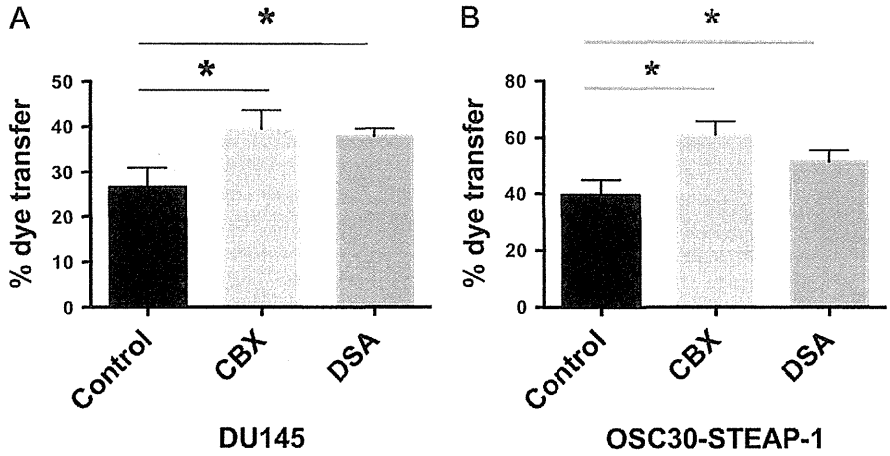

Fig. 6 – Inhibition of gap junctional communication augments STEAP-1-mediated intercellular communication. Calcein AM-loaded DU145 cells (A) or calcein AM-loaded OSC30-STEAP-1 cells (B) were treated with the gap junction inhibitors carbenoxolone (CBX) and deoxyl stearic acids (DSA). The cells were layered over acceptor cells loaded with dextran–Texas red at a ratio of 1:3. Cells were incubated at 37 °C for 3 h. Percentage transfer was calculated as the fraction of cells that accepted the green dye (yellow/orange cells) in the total population of acceptor cells (yellow/orange and red cells). Statistical analysis using Student's *t* tests (two-tailed) for percentage dye transfer shows $P<0.05$ for CBX and DSA versus Control in DU145 cells and $P<0.05$ for CBX and DSA versus Control in OSC30-STEAP-1 cells. Data are representative of three independent experiments.

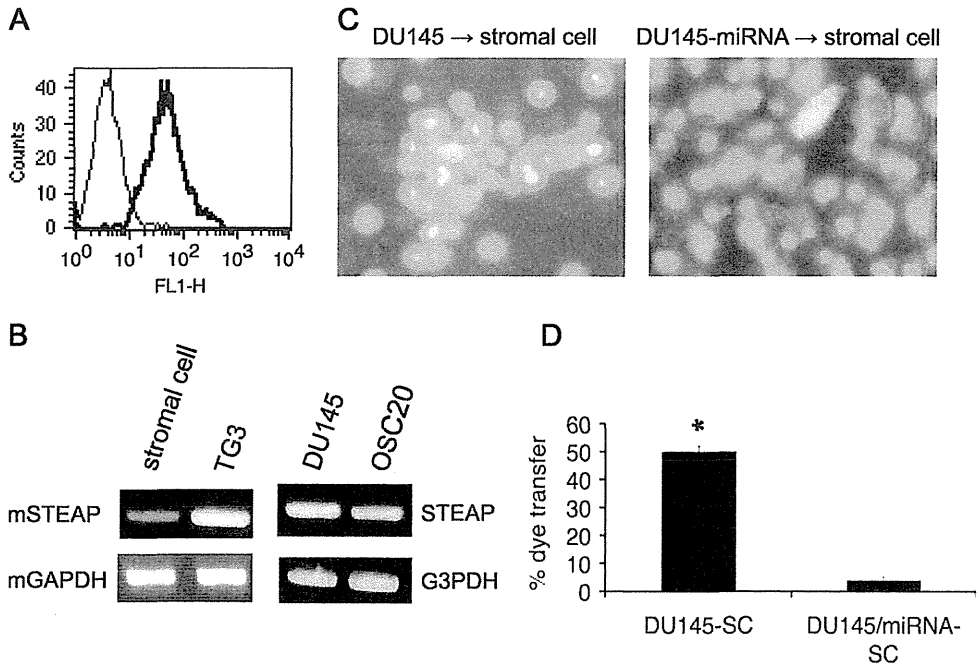

Fig. 7 – STEAP-1 is required for intercellular communication between cancer cells and stromal cells. (A) The isolated stromal cells were analyzed for cell-surface expression of H-2K^d (H-2K^d, thick line; isotype control, thin line). (B) RT-PCR analysis demonstrated that stromal cells express murine *STEAP-1* mRNA. As a positive control, murine fibrosarcoma cell line TG3 expressed murine *STEAP-1* and DU145 and OSC20 expressed human *STEAP-1*. (C) Accepter cells (stromal cells isolated from DU145 tumor mass) were loaded with dextran–Texas red and donor cells (DU145) were loaded with calcein AM and mixed 1:3 to allow intercellular communication to occur as manifested by the appearance of the yellow/orange color (see Materials and methods). Representative pictures were taken from DU145–stromal cells, DU145-miRNA–stromal cells. (D) Percentage transfer was calculated as the fraction of cells that accepted the green dye (yellow/orange cells) in the total population of acceptor cell (yellow/orange and red cells). Transfer was measured by counting the number of cells in five different fields using fluorescence microscopy. Statistical analysis using Student's *t* tests (two-tailed) for percentage dye transfer shows $P<0.01$ for DU145–stromal cells versus DU145-miRNA–stromal cells. Data are representative of three independent experiments.

donor cells loaded with calcein AM and stromal cells, which were isolated from DU145 tumor mass, as acceptor cells loaded with dextran–Texas red were mixed. Extensive dye transfer was observed in almost all cells in cultures where between DU145 cancer cells and stromal cells (Fig. 7C). In contrast, dye transfer from DU145-miRNA to stromal cells was infrequently observed. As shown in Fig. 7D, the expression of STEAP-1 on the tumor cell significantly affected the intercellular communication. These results suggested that transfer of the small molecules from tumor cells to stromal cells was dependent on the STEAP-1 expressed by the tumor cells. Moreover, these data may suggest that tumor-derived substances transferred by STEAP-1 are essential for stromal cell recruitment and proliferation at the tumor microenvironment.

Discussion

In this study, we found that STEAP-1 played an important role for tumor progression in vivo and knockdown of STEAP-1 expression on tumor cells caused antitumor effect through disruption of intercellular communication of small molecules between tumor cells and adjacent tumor-associated stromal cells. STEAP-1 is a member of the metalloreductase family that lacks the NH_2-terminal oxidoreductase domain and currently has no defined enzymatic function [16,17]. It has been demonstrated that STEAP-1 is expressed in the normal prostate tissues but it is highly expressed in human prostate cancer tissue [1]. STEAP-1 has also been detected in various types of cancer, such as colon, bladder, ovarian, and pancreatic cancer cell lines, reinforcing the idea that this gene may be up-regulated in transformed cells [2,4–6]. In addition, according to the STEAP-1 structure, it is predicted to act as a transporter or an adhesion molecule. In fact, Challita-Eid et al. have shown that blocking STEAP-1 using mAb against STEAP-1 inhibited intercellular communication in vitro and in vivo, resulting in tumor growth retardation [6].

The Cx family member has been shown to play a central role in the intercellular communication that plays a fundamental function in the regulation of cell and tissue homeostasis. It is known that Cx family member is downregulated during the course of tumor progression [18]. In accordance with this, we observed that DU145 cells did not express Cx43 on the cell surfaces by immunohistochemistry. In addition, we did not detect Cx32 mRNA in DU145 cells. Moreover, inhibition of gap junction-mediated communication using inhibitors did not inhibit STEAP-1-mediated intercellular communication. Therefore, we assumed that some undefined cell-surface molecules responsible for the transport of small molecules might exist. Our data suggest that

STEAP-1 plays a crucial role in the intercellular communication between tumor cells and surrounding stromal cells.

The role of cell–cell communication in cancer pathogenesis has been gaining attention [8,19,20]. Cellular communication facilitates the intercellular exchange of small molecular weight solutes, such as nutrients, metabolites, electrolytes, and second messenger from distant blood vessels, thus supporting tumor growth. Thus, cell–cell communication in the ability of tumor cells to invade and metastasize has been focused [20,21]. Intercellular communication between cancer cell and stromal cells has been shown to increase tumor invasion and to increase vascular endothelial growth factor (VEGF) secretion, leading to vascular tube formation [22]. We have established stable STEAP-knockdown tumor cells such as DU145 and OSC20 using miRNA-mediated RNA interference. Tumor cell proliferation did not alter in mock miRNA-transfected cells and STEAP-1 knockdown cells in vitro. However, STEAP-1 knockdown tumor cells of OSC20 showed the in vivo tumor growth retardation compared with parental cells or mock-transfected cells. In contrast, OSC30 transfected with STEAP-1 cDNA showed augmented tumor growth in vivo compared with wild type OSC30, which is STEAP-1 negative carcinoma line. These notions took us to examine the role of STEAP-1 for the interaction of tumor cells and surrounding stromal cells within the solid tumor microenvironment. Using the dye transfer assay, we showed that cancer cells, which expressed STEAP-1, induce significant dye transport between cancer cells and stromal cells. In clear contrast, dye transfer was diminished when STEAP-1-knockdown OSC20 tumor cells were used. Moreover, inhibition of tumor growth by knockdown of STEAP-1 of tumor cells and its intercellular transport function suggest a potential role for STEAP-1 transport function and its involvement in tumor cell growth in vivo. Taken together, our data suggested that the transfer of small molecular weight solutes released from tumor via STEAP-1 to stromal cells was required for tumor growth in vivo.

Recent reports demonstrated that tumor-associated stromal cells played a crucial role for tumor growth, invasion and metastasis [23–25]. It has been demonstrated that stromal cells, particularly fibroblasts, support tumor cells in invasion of surrounding tissue for access to the vascular system [23,26]. In addition, during carcinogenesis, stromal fibroblasts undergo certain changes in concert with their neoplastic neighbors, leading to a tumor-associated state. Experimental and clinical studies have revealed that tumor stromal cells can be derived from bone marrow (BM)-derived progenitor cells, such as mesenchymal stem cells (MSCs), which can be mobilized into the circulation and incorporate into tumor microenvironments [27]. Recent report demonstrated that MSCs expressed STEAP-1, indicating that tumor-associated macrophages and fibroblasts might also express STEAP-1 molecules. Many observations indicate that, in the tumor microenvironment, MSCs have several tumor growth promoting functions, including expression of growth factors, promotion of tumor vessel formation and creation of tumor stem cell niches. In fact, we have demonstrated that DU145 tumor-derived stromal cells expressed STEAP-1 molecules and was involved in the intercellular communication between DU145 cells and their stromal cells, leading to augmentation of tumor growth in vivo. Therefore, knockdown of STEAP-1 expression on tumor cells or administration of monoclonal antibody against STEAP-1 holds the new aspects for cancer therapy.

The predicted structure of STEAP-1 may indicate the function in tumor cell growth. STEAP-1 contains a heme-binding domain called apoptosis, cancer and redox associated transmembrane domain, which is present in a structurally related family identified recently to include members of the STEAP family, such as STEAP-2, STEAP-3 and STEAP-4 [16,17,28]. The heme-binding domain function present in this family may facilitate electron transfer and thereby alter cell growth and metabolism as has been shown for the bacterial proteins. The role of this structural feature of STEAP-1 in its intercellular transport function remains to be explored. In addition, it is very important to clarify whether their extracellular domains interact with other molecules expressed on the adjacent cells or not. Furthermore, it is necessary to determine which molecules are interacted with the intracellular domains of STEAP-1. These extracellular and intracellular protein–protein interactions may hold the key roles for intercellular communication.

Although we demonstrated the functional role for STEAP-1 between cancer cells and stromal cells in vitro, it will next be crucial, although challenging, to determine the in vivo relevance to understand the physiological roles played by STEAP-1 between these cells. It is equally important to note key questions that remain to be clarified. First, one must determine the molecular identities and quantities of molecules transmitted via STEAP-1, which are required for tumor development. Second, it is important to determine whether other channel molecules including connexins are involved in the STEAP-1-mediated small molecule transport.

In summary, our results identified a STEAP-1-mediated mechanism for intercellular communication of small molecules, which is required for promoting tumor progression. We believe that the present study provides a new avenue for understanding the roles played by STEAP-1 in biological activities of tumor cells and tumor stromal cells, and the development of new therapeutic strategy for tumors. The challenge for the future is to identify the factors that participate in this communication and their mechanisms of action.

Conflict of interest

The authors have no conflict of interest.

Acknowledgments

We thank Dr. H. Ikeda (Hokkaido Red Cross Blood Center) for generous help to our study. This work was supported in part by program for developing the supporting system for upgrading the education and research from the Ministry of Education, Culture, Sports, Science and Technology. The authors have no conflicting financial interests in this work.

REFERENCES

[1] R.S. Hubert, I. Vivanco, E. Chen, S. Rastegar, K. Leong, S.C. Mitchell, R. Madraswala, Y. Zhou, J. Kuo, A.B. Raitano, A. Jakobovits, D.C. Saffran, D.E. Afar, STEAP: a prostate-specific cell-surface antigen highly expressed in human prostate tumors, Proc. Nat. Acad. Sci. USA 96 (1999) 14523–14528.

[2] D.A. Rodeberg, R.A. Nuss, S.F. Elsawa, E. Celis, Recognition of six-transmembrane epithelial antigen of the prostate-expressing tumor cells by peptide antigen-induced cytotoxic T lymphocytes, Clin. Cancer Res. 11 (2005) 4545–4552.
[3] A. Machlenkin, A. Paz, E. Bar Haim, O. Goldberger, E. Finkel, B. Tirosh, I. Volovitz, E. Vadai, G. Lugassy, S. Cytron, F. Lemonnier, E. Tzehoval, L. Eisenbach, Human CTL epitopes prostatic acid phosphatase-3 and six-transmembrane epithelial antigen of prostate-3 as candidates for prostate cancer immunotherapy, Cancer Res. 65 (2005) 6435–6442.
[4] P.M. Alves, O. Faure, S. Graff-Dubois, S. Cornet, I. Bolonakis, D.A. Gross, I. Miconnet, S. Chouaib, K. Fizazi, J.C. Soria, F.A. Lemonnier, K. Kosmatopoulos, STEAP, a prostate tumor antigen, is a target of human CD8+ T cells, Cancer Immunol. Immunother. 55 (2006) 1515–1523.
[5] H. Kobayashi, T. Nagato, K. Sato, N. Aoki, S. Kimura, M. Murakami, H. Iizuka, M. Azumi, H. Kakizaki, M. Tateno, E. Celis, Recognition of prostate and melanoma tumor cells by six-transmembrane epithelial antigen of prostate-specific helper T lymphocytes in a human leukocyte antigen class II-restricted manner, Cancer Res. 67 (2007) 5498–5504.
[6] P.M. Challita-Eid, K. Morrison, S. Etessami, Z. An, K.J. Morrison, J.J. Perez-Villar, A.B. Raitano, X.C. Jia, J.M. Gudas, S.B. Kanner, A. Jakobovits, Monoclonal antibodies to six-transmembrane epithelial antigen of the prostate-1 inhibit intercellular communication in vitro and growth of human tumor xenografts in vivo, Cancer Res. 67 (2007) 5798–5805.
[7] N.M. Kumar, N.B. Gilula, The gap junction communication channel, Cell 84 (1996) 381–388.
[8] K. Ko, P. Arora, W. Lee, C. McCulloch, Biochemical and functional characterization of intercellular adhesion and gap junctions in fibroblasts, Am. J. Physiol. Cell Physiol. 279 (2000) C147–C157.
[9] P.P. Mehta, C. Perez-Stable, M. Nadji, M. Mian, K. Asotra, B.A. Roos, Suppression of human prostate cancer cell growth by forced expression of connexin genes, Dev. Genet. 24 (1999) 91–110.
[10] M. Hernandez, Q. Shao, X.J. Yang, S.P. Luh, M. Kandouz, G. Batist, D.W. Laird, M.A. Alaoui-Jamali, A histone deacetylation-dependent mechanism for transcriptional repression of the gap junction gene cx43 in prostate cancer cells, Prostate 66 (2006) 1151–1161.
[11] G. Carruba, M.M. Webber, S.T. Quader, M. Amoroso, L. Cocciadiferro, F. Saladino, J.E. Trosko, L.A. Castagnetta, Regulation of cell-to-cell communication in non-tumorigenic and malignant human prostate epithelial cells, Prostate 50 (2002) 73–82.
[12] T. Kurotaki, Y. Tamura, G. Ueda, J. Oura, G. Kutomi, Y. Hirohashi, H. Sahara, T. Torigoe, H. Hiratsuka, H. Sunakawa, K. Hirata, N. Sato, Efficient cross-presentation by heat shock protein 90-peptide complex-loaded dendritic cells via an endosomal pathway, J. Immunol. 179 (2007) 1803–1813.
[13] L. Zhang, Y.M. Li, Y.H. Jing, S.Y. Wang, Y.F. Song, J. Yin, Protective effects of carbenoxolone are associated with attenuation of oxidative stress in ischemic brain injury, Neurosci. Bull. 29 (2013) 311–320.
[14] T. Toyofuku, M. Yabuki, K. Otsu, T. Kuzuya, M. Hori, M. Tada, Intercellular calcium signaling via gap junction in connexin-43-transfected cells, J. Biol. Chem. 273 (1998) 1519–1528.
[15] S.W. Lee, C. Tomasetto, D. Paul, K. Keyomarsi, R. Sager, Transcriptional downregulation of gap-junction proteins blocks junctional communication in human mammary tumor cell lines, J. Cell Biol. 118 (1992) 1213–1221.
[16] L. Sanchez-Pulido, A.M. Rojas, A. Valencia, A.C. Martinez, M.A. Andrade, ACRATA: a novel electron transfer domain associated to apoptosis and cancer, BMC Cancer 4 (2004) 98.
[17] R.S. Ohgami, D.R. Campagna, A. McDonald, M.D. Fleming, The Steap proteins are metalloreductases, Blood 108 (2006) 1388–1394.
[18] H. Tsai, J. Werber, M.O. Davia, M. Edelman, K.E. Tanaka, A. Melman, G.J. Christ, J. Geliebter, Reduced connexin 43 expression in high grade, human prostatic adenocarcinoma cells, Biochem. Biophys. Res. Commun. 227 (1996) 64–69.
[19] R. Govindarajan, S. Zhao, X.H. Song, R.J. Guo, M. Wheelock, K.R. Johnson, P.P. Mehta, Impaired trafficking of connexins in androgen-independent human prostate cancer cell lines and its mitigation by alpha-catenin, J. Biol. Chem. 277 (2002) 50087–50097.
[20] W. Zhang, C. Nwagwu, D.M. Le, V.W. Yong, H. Song, W.T. Couldwell, Increased invasive capacity of connexin43-overexpressing malignant glioma cells, J. Neurosurg. 99 (2003) 1039–1046.
[21] J.H. Lin, T. Takano, M.L. Cotrina, G. Arcuino, J. Kang, S. Liu, Q. Gao, L. Jiang, F. Li, H. Lichtenberg-Frate, S. Haubrich, K. Willecke, S.A. Goldman, M. Nedergaard, Connexin 43 enhances the adhesivity and mediates the invasion of malignant glioma cells, J. Neurosci. 22 (2002) 4302–4311.
[22] W. Zhang, J.A. DeMattia, H. Song, W.T. Couldwell, Communication between malignant glioma cells and vascular endothelial cells through gap junctions, J. Neurosurg. 98 (2003) 846–853.
[23] L.W. Qian, K. Mizumoto, N. Maehara, K. Ohuchida, N. Inadome, M. Saimura, E. Nagai, K. Matsumoto, T. Nakamura, M. Tanaka, Co-cultivation of pancreatic cancer cells with orthotopic tumor-derived fibroblasts: fibroblasts stimulate tumor cell invasion via HGF secretion whereas cancer cells exert a minor regulative effect on fibroblasts HGF production, Cancer Lett. 190 (2003) 105–112.
[24] P. Micke, A. Ostman, Tumour-stroma interaction: cancer-associated fibroblasts as novel targets in anti-cancer therapy?, Lung Cancer 45 (Suppl. 2) (2004) S163–S175.
[25] Y. Matsuo, N. Ochi, H. Sawai, A. Yasuda, H. Takahashi, H. Funahashi, H. Takeyama, Z. Tong, S. Guha, CXCL8/IL-8 and CXCL12/SDF-1alpha co-operatively promote invasiveness and angiogenesis in pancreatic cancer, Int. J. Cancer 124 (2009) 853–861.
[26] C. Werth, D. Stuhlmann, B. Cat, H. Steinbrenner, L. Alili, H. Sies, P. Brenneisen, Stromal resistance of fibroblasts against oxidative damage: involvement of tumor cell-secreted platelet-derived growth factor (PDGF) and phosphoinositide 3-kinase (PI3K) activation, Carcinogenesis 29 (2008) 404–410.
[27] F.A. Fierro, W.D. Sierralta, M.J. Epunan, J.J. Minguell, Marrow-derived mesenchymal stem cells: role in epithelial tumor cell determination, Clin. Exp. Metastasis 21 (2004) 313–319.
[28] M.D. Knutson, Steap proteins: implications for iron and copper metabolism, Nutr. Rev. 65 (2007) 335–340.

Biochemical and Biophysical Research Communications 439 (2013) 96–102

Contents lists available at ScienceDirect

Biochemical and Biophysical Research Communications

journal homepage: www.elsevier.com/locate/ybbrc

Small proline-rich protein-1B is overexpressed in human oral squamous cell cancer stem-like cells and is related to their growth through activation of MAP kinase signal

Yoshitaka Michifuri [a,b], Yoshihiko Hirohashi [a,*], Toshihiko Torigoe [a,*], Akihiro Miyazaki [b], Jyunki Fujino [a,b], Yasuaki Tamura [a], Tomohide Tsukahara [a], Takayuki Kanaseki [a], Junichi Kobayashi [b], Takanori Sasaki [a,b], Akari Takahashi [a], Kenji Nakamori [b], Akira Yamaguchi [b], Hiroyoshi Hiratsuka [b], Noriyuki Sato [a]

[a] Department of Pathology, Sapporo Medical University School of Medicine, South-1 West-17, Chuo-ku, Sapporo 060-8556, Japan
[b] Department of Oral Surgery, Sapporo Medical University School of Medicine, South-1 West-17, Chuo-ku, Sapporo 060-8556, Japan

ARTICLE INFO

Article history:
Received 3 August 2013
Available online 13 August 2013

Keywords:
Oral cancer
Cancer stem cell
SPRR1B
RASSF4
ALDEFLUOR assay

ABSTRACT

Cancer stem-like cells (CSCs)/cancer-initiating cells (CICs) are considered to be essential for tumor maintenance, recurrence and metastasis. Therefore, eradication of CSCs/CICs is essential to cure cancers. However, the molecular mechanisms of CSCs/CICs are still elusive. In this study, we investigated the molecular mechanism of the cell growth of oral CSCs/CICs. Oral CSCs/CICs were isolated as aldehyde dehydrogenase 1 bright ($ALDH1^{br}$) cells by the ALDEFLUOR assay. *Small proline-rich protein-1B* (*SPRR1B*) gene was shown to be overexpressed in $ALDH1^{br}$ cells by a cDNA microarray and RT-PCR. SPRR1B was shown to have a role in cell growth and maintenance of $ALDH1^{br}$ cells by SPRR1B overexpression and knockdown experiments. To elucidate the molecular mechanism by which SPRR1B regulates cell growth, further cDNA microarray analysis was performed using SPRR1B-overexpressed cells and cells with SPRR1B knocked down by siRNA. Expression of the tumor suppressor gene Ras association domain family member 4 (*RASSF4*) was found to be suppressed in SPRR1B-overexpressed cells. On the other hand, the expression of *RASSF4* was enhanced in cells in which SPRR1B expression was knocked down by SPRR1B-specific siRNA. RASSF4 has an RA (Ras association) domain, and we thus hypothesized that RASSF4 modulates the MAP kinase signal downstream of the Ras signal. MAP kinase signal was activated in SPRR1B-overexpressed cells, whereas the signal was suppressed in SPRR1B knocked down cells. Taken together, the results indicate that the expression of SPRR1B is upregulated in oral CSCs/CICs and that SPRR1B has a role in cell growth by suppression of RASSF4.

1. Introduction

Head and neck cancer including oral squamous cell carcinoma (OSCC) is the sixth most common cancer worldwide and is a serious growing health problem all over the world [1]. Despite recent progress in treatments, survival rates of patients with the disease have not greatly improved. The poor prognosis is due to resistance to treatment, recurrence and distant metastasis.

The theory of cancer stem-like cells/cancer-initiating cells (CSCs/CICs) has recently emerged [2]. This theory is based on the idea that cancers are composed of heterogeneous cell populations and only a small fraction of cancer cells can give rise to a tumor again. Therefore, CSCs/CICs are thought to be responsible for recurrence and distant metastasis, and, importantly, CSCs/CICs have been shown to be resistant to chemotherapy and radiotherapy [3]. CSCs/CICs were initially reported in hematopoietic malignancies and later in solid tumors [4,5]. CSCs/CICs have also been isolated from primary head and neck squamous cell carcinomas (HNSCC) using the CSC/CIC marker CD44, which is a common CSC/CIC marker [6,7]. $CD44^{+}$ cells were also reported to express chemoresistance genes, including *ABCB1*, *ABCG2* and *CYP2C8* [8].

The aldehyde dehydrogenase (ALDH) family of enzymes is comprised of cytosolic isoenzymes that oxidize intracellular aldehydes and contribute to the oxidation of retinol to retinoic acid in early stem cell differentiation [9]. High ALDH1 activity has been used to isolate normal hematopoietic and central nervous system stem cells [10–13]. ALDH1 activity has also been found in stem cells

Abbreviations: CSC, cancer stem-like cell; CIC, cancer-initiating cell; OSCC, oral squamous cell carcinoma; SPRR1B, small proline-rich protein-1B; RASSF4, ras association domain family member 4; NOD/SCID, non-obese diabetic/severe combined immunodeficiency.

* Corresponding authors.
E-mail addresses: hirohash@sapmed.ac.jp (Y. Hirohashi), torigoe@sapmed.ac.jp (T. Torigoe).

0006-291X/$ - see front matter © 2013 Elsevier Inc. All rights reserved.
http://dx.doi.org/10.1016/j.bbrc.2013.08.021

derived from hematopoietic malignancies including multiple myeloma and acute myeloid leukemia [12,14]. Ginestier et al. successfully isolated breast CSCs/CICs by using ALDH1 activity for the first time [15]. Chen et al. reported isolation of CSCs/CICs from head and neck squamous cell carcinoma (HNSCC) by using ALDH1 activity [16]. These reports indicate that ALDH expression may be an important new marker for the isolation of CSCs/CICs.

In this study, we isolated oral CSCs/CICs by the ALDEFLUOR assay and isolated a novel oral CSC/CIC-specific genes. One of the oral CSC/CIC-specific genes was *small proline-rich protein-1B (SPRR1B)*, and we analyzed the molecular mechanisms of SPRR1B in oral CSCs/CICs.

2. Materials and methods

2.1. Cell lines and cell culture

Human oral squamous cell carcinoma (OSCC) cell lines, OSC19, OSC20, OSC30, OSC40, OSC70 and POT1, were established in our laboratory (Table S1). The OSCC cell line HSC-2 was purchased from the Human Science Research Resources Bank (HSRRB, Osaka, Japan). The OSCC cell line SAS was obtained from the Institute of Development, Aging and Cancer, Tohoku University (Tohoku, Japan). All of these cell lines were cultured in RPMI-1640 medium (Sigma–Aldrich, Tokyo, Japan) supplemented with 10% fetal bovine serum (Life Technologies Japan, Tokyo, Japan) at 37 °C in a humidified 5% CO_2 atmosphere.

2.2. Isolation and culture of OSCC-derived ALDH1^{br} cells

Identification of aldehyde dehydrogenase 1 (ALDH1)-positive OSCC cells was carried out using the ALDEFLUOR assay (StemCell Technologies, Durham, NC, USA) and fluorescence-activated cell sorting as described previously [15,17,18].

2.3. Reverse transcriptase PCR (RT-PCR)

RT-PCR analysis was performed as described previously [19]. The PCR mixture was initially incubated at 98 °C for 2 min, followed by 35 cycles of denaturing at 98 °C for 15 s, annealing at 58 °C for 30 s, and extension at 72 °C for 30 s. Primer pairs used for RT-PCR analysis were 5-CCAGTTCTAAGGGACCATACAGA-3′ and 5′-CTCCTTGGTTTTGGGGATG-3′ for *SPRR1B* with an expected PCR product size of 181 base pairs (bp), 5′-CATGATGGAGACG GAGCTGA-3′ and 5′-ACCCCGCTCGCCATGCTATT-3′ for *SOX2* with an expected PCR product size of 410 bp, 5′-TGGAGAAGGAGAAGCT GGAGCAAAA-3′ and 5′-GGCAGATGGTCGTTTGGCTGAATA-3′ for *POU5F1* with an expected PCR product size of 163 bp, 5′-TGTTAGC

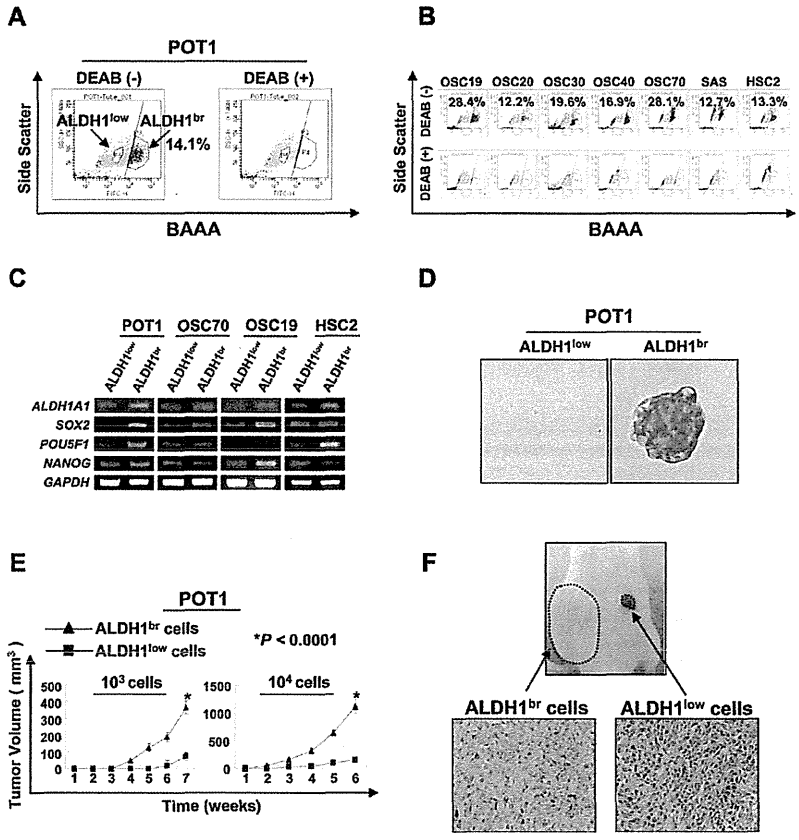

Fig. 1. Isolation of CSCs/CICs from OSCC cells by ALDEFLUOR assay. (A, B) ALDH1^{br} cells were isolated using several OSCC cell lines (POT1, OSC19, OSC20, OSC30, OSC40, OSC70, SAS and HSC2). Percentage represents the proportions of ALDH1^{br} cells. (C) RT-PCR of stem cell markers. ALDH1^{br} and ALDH1^{low} cells derived from POT1, OSC70, OSC19 and HSC2 cells were examined for expression of stem cell markers (*SOX2*, *POU5F1* and *NANOG*). *GAPDH* was used as an internal control. (D) Representative picture of tumor sphere. ALDH1^{br} and ALDH1^{low} cells derived from POT1 cells were cultured in DMEM/F12 media containing EGF and bFGF. After 2 weeks of culture *in vitro*, a picture of a tumor sphere was taken. (E) Tumor formation ability of POT1 ALDH1^{br} and ALDH1^{low} cells. ALDH1^{br} and ALDH1^{low} cells derived from POT1 cells were inoculated into the backs of NOD/SCID mice subcutaneously with serial dilution (10^2–10^5). Graphs show the tumor growth curves of ALDH1^{br} (closed triangle) – and ALDH1^{low} (closed circle) – injected groups with injections of 10^3 and 10^4 cells. Data represent means ± SD. Differences between ALDH1^{br} cells and ALDH1^{low} cells were examined for statistical significance using Student's *t*-test. *$P < 0.0001$. (F) Histology of ALDH1^{br} cell-derived and ALDH1^{low} cell-derived tumors. Tumors derived from POT1 ALDH1^{br} cells and POT1 ALDH1^{low} cells were stained by hematoxylin and eosin. Magnification, ×200.

Table 1
Tumorigenicity of POT1-ALDH1^{br} and ALDH1^{low} cells at 5-weeks after inoculation into NOD/SCID mice.

		Cell numbers of inoculation			
Population		100	1000	10,000	10,00,00
ALDH1^{br}	Incidence	0% (0/5)	80% (4/5)	100% (5/5)	n.d.
	Volumes (mm^3)	–	127.0 ± 18.6*	645.0 ± 35.7*	
ALDH1^{low}	Incidence	0% (0/5)	40% (2/5)	60% (3/5)	100% (5/5)
	Volumes (mm^3)	–	19.0 ± 26.1*	97.0 ± 24.4*	570.0 ± 45.6

Data shown are for xenografted samples.
NOD/SCID mice were injected with live ALDH1^{br} and ALDH1^{low} cells isolated by ALDEFLUOR assay and mixed with matrigel.
Numbers indicate the ratio of tumour incidence relative to the number of injections.
* $P < 0.0001$.

TGATGCCGACTTG-3′ and 5′-TTCTTAGCCCGCTCAACACT-3′ for *ALDH1A1* with an expected PCR product size of 154 bp, 5′-GCTGAG ATGCCTCACACGGAG-3′ and 5′-TCTGTTTCTTGACCGGGACCTTGTC-3′ for *NANOG* with an expected PCR product size of 161 bp, 5′-ACCGTGAGG AAGAAGGGACT-3′ and 5′-CCTTTAGAGGGCAGCTAGG C-3′ for *RASSF4* with an expected PCR product size of 156 bp and 5′-ACCACAGTCCATGCCATCAC-3′ and 5′-TCCACCACCCTGTTGCTG-TA-3′ for *glyceraldehyde-3-phosphate dehydrogenase (GAPDH)* with an expected product size of 452 bp. *GAPDH* was used as an internal control.

2.4. Gene expression profiling using cDNA microarrays

The total RNAs from ALDH1^{br} cells were labeled with Cy5 dye and those from ALDH1^{low} cells were labeled with Cy3 dye and were hybridized to a 29138-spot Human Panorama Micro Array (Sigma–Aldrich) for 16 h at 45 °C. The intensities of Cy5 and Cy3 fluorescence were measured with a GenePix 4000B scanner (Axon Instruments, Austin, TX) and were analyzed with GenePix Pro 5.0 software (Axon Instruments). Global normalization of the resultant data was carried out using Excel 2004 (Microsoft, Redmond, WA). A dye-swap experiment (labeling ALDH1^{br} and ALDH1^{low} cells with Cy3 and Cy5, respectively) was also performed. An average ratio of more than 2.0, reproducible in two experiments, was determined to indicate differential upregulation in ALDH1^{br} cells.

2.5. Xenograft transplantation

Xenogtaft transplatation was performed as described previously [17,18]. Sorted ALDH1^{br} and ALDH1^{low} cells from POT1 cells were collected and re-suspended at concentrations of 1×10^2 to 1×10^5 cells per 100 μl of PBS and then mixed with 100 μl of Matrigel (BD Biosciences).

2.6. siRNAs and transfection

SPRR1B and *RASSF4* specific small interfering RNA (siRNA) were desined and synthesised using the BLOCK-it RNAi designer system (Life Technologies). Cells were seeded at 50% confluence, and transfections were carried out using Lipofectamine RNAi max (Life Technologies) according to the manufacturer's instructions. Control siRNAs were obtained from Life technologies.

2.7. SPRR1B stable transformant

Full-length *SPRR1B* cDNA was amplified from cDNA of POT1 with PCR using KOD-Plus DNA polymerase (Toyobo, Osaka, Japan). The PCR product was inserted into pMXs-puro expression vector (a kind gift from Prof. T Kitamura, Tokyo, Japan). Genes were transduced by a retrovirus packaging cell PLAT-A (a kind gift from Prof. T Kitamura, Tokyo, Japan) as described previously [20].

2.8. Western blot

Western blotting was performed as described previously [19]. For detection of ERK and phosphorylated ERK, rabbit anti-ERK polyclonal antibody (K-23; 1:200 dilution; Santa Cruz Biotech.) and rabbit anti-phospho-p44/42 MAPK (Erk1/2) (Thr 202/Tyr 204) monoclonal antibody (D13.14.4E, 1:2000 dillution; Cell Signaling Tech.) were used.

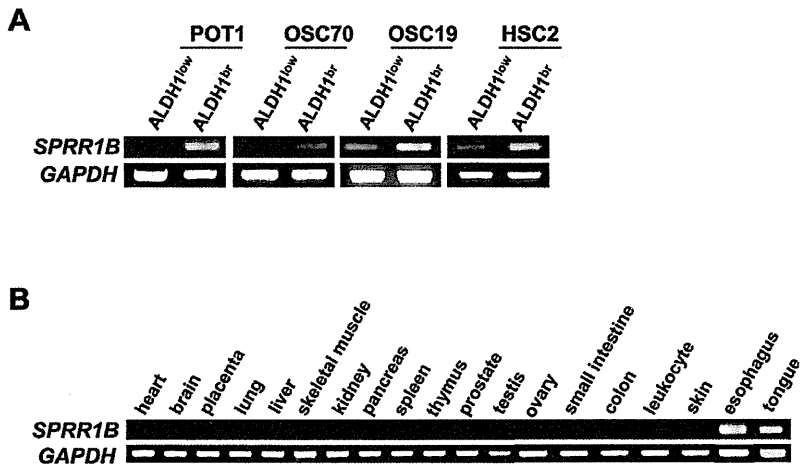

Fig. 2. Expression of *SPRR1B* in various oral cancer cell lines and human normal adult tissues. (A) Expression of *SPRR1B* in various oral cancer cell lines. *SPRR1B* expression was assessed by RT-PCR using ALDH1^{br} and ALDH1^{low} cells derived from POT1, OSC70, OSC19 and HSC2 cells. *GAPDH* was used as an internal control. (B) Expression of *SPRR1B* in normal adult tissues. *SPRR1B* expression was assessed by RT-PCR using the heart, brain, placenta, lung, liver, skeletal muscle, kidney, pancreas, spleen, thymus, prostate, testis, ovary, small intestine, colon, leukocytes, skin, esophagus and tongue. *GAPDH* was used as an internal control.